INCLUSIVE REACTIONS AT CONVENTIONAL ACCELERATORS

By Y. Goldschmidt-Clermont

CERN, Geneva*

(Presented at the XIII Cracow School of Theoretical Physics, Zakopane, June 1–12, 1973)

Some characteristic features of inclusive spectra obtained in experiments at conventional accelerators are reviewed. Discussed are particle multiplicities, longitudinal momenta in the reactions $K^+p \to K^0 + X$, $K^+p \to K^{*+} + X$, transverse momenta.

1. Introduction, notations and plan

1.1. Introduction

Most theoretical predictions on inclusive reactions are relative to the asymptotic region of very high incident momenta: the basic conjectures of scaling, introduced by Feynman [1], and of limiting fragmentation presented by Benecke, Chou, Yang and Yen [2] should be tested at the highest available energies. Thus the exciting results obtained at the ISR steal the show. What can be learned with conventional accelerators? This question is answered, in the present lectures, by some typical examples. There exist indeed several topics which may be specifically studied with conventional accelerators, some of them are as follows:

The dependence on the nature of the incident particle. At present, the ISR allows only the study of pp collisions. What happens with incident $\pi^\pm$, $K^\pm$, $\bar{p}$? Some examples of characteristic differences are shown in Sect. 2 and 4.

The approach to scaling. The theorem of Mueller [3] relating the inclusive cross-section to the discontinuity, at zero momentum transfer, of a 3-particle elastic collision, the description of this amplitude in terms of exchanged trajectories has extended to inclusive reactions the main concepts of Regge phenomenology. The Regge and Pomeron trajectories, factorization, duality, lead to some definite predictions at energies where scaling is not yet reached. Early scaling (*i. e.* scaling at low energy) or early limiting fragmentation is predicted for some combinations of quantum numbers of the particles studied [4]. Examples are given in Sect. 3.

* Address: CERN, 1211 Geneva 23, Switzerland.

The relations between inclusive and exclusive reactions. A complete knowledge of one, two, ..., n particle exclusive reactions would give a full information on high energy collisions, just as well as a full knowledge of all contributing exclusive reactions. Both complete descriptions are equally unattainable today, but also both approaches are complementary. An interesting review of this complementarity is given by Kittel [5]. Here, only a few topics are briefly mentioned, in particular that of resonance production (Sect. 3).

Correlations. At accelerator energies, the correlations studied up to now seem to have brought but little new information, in addition to what is known from the study of spectra of single particles and resonances. The experimental results are summarized by Morrison [6], and are not repeated here. Yet, there remain unexplained properties, such as the GGLP effect [7]. It is to be hoped that this paradoxical situation may be improved by further, more differential studies, for which the bubble chamber investigations at conventional accelerators are probably best suited.

Some special classes of inclusive reactions, such as antiproton annihilation or, perhaps more generally baryon exchange, indicate peculiar properties (Sect. 2 and 4) that need deeper investigation.

Inclusive production of resonances, readily detectable with bubble chambers, such as K^*, Δ^{++} *etc.* and observation of their decay, make it possible to determine the spin alignment and to obtain more detailed information on the mechanism of inclusive reactions. An example is given in Sect. 3.

A vigorous theoretical activity, illustrated by many of the lectures at this School, explore the properties of numerous models of inclusive reactions and multiple particle production. Dependences on incident energy, incident particle *etc.*, obtainable only with conventional accelerators, may perhaps provide crucial tests. Other tests may arise from the detailed differential information obtainable, for instance, in bubble chamber experiments. For the present, there exist many models which have not yet been fully tested, but also a wealth of experimental data which have not been used. It is hoped that some of the experimental regularities displayed by the data presented here, may stimulate further informative comparisons with theory, and further experimentation.

1.2. Notations and terminology

An exclusive reaction, produced by an incident projectile a on a target b, and denoted by $a+b \to c+X$, where X represents any and every possible combination of particles, is kinematically similar to a two-body reaction. Writing for particle α of mass m_α the four-momentum $p_\alpha^\mu = (E_\alpha, \boldsymbol{p}_\alpha)$, $p_\alpha = |\boldsymbol{p}_\alpha|$, the square of the total energy in the CM is $s = (p_a + p_b)^2$. In addition, two variables suffice to describe the final state when unpolarized projectile and target secure azimuthal symmetry. Usual choices of sets are as follows.

In the CM, the two projections of the momentum $\boldsymbol{p}_c$, the longitudinal p_L along the initial projectile direction, and the transverse p_T. (The index c will be written only when needed to avoid confusion.)

In the target frame of reference (laboratory) the longitudinal momentum $p_L^{(t)}$ and transverse momentum p_T of particle c — correspondingly in the projectile frame $p_L^{(p)}$, p_T.

In the CM, the Feynman variable $x = p_L/p_{Lmax}$, also called reduced longitudinal momentum, and p_T. Here, p_{Lmax} is the maximum value of p_L allowed by kinematics. The asymptotic value of p_{Lmax} for $s \to \infty$ is $\frac{1}{2}\sqrt{s}$, some authors chose $x = 2p_L/\sqrt{s}$ even at finite energies when $p_{Lmax} \neq \frac{1}{2}\sqrt{s}$.

The mass M of X (missing mass) and 4-momentum transfer $t = (p_a - p_c)^2$ between the projectile a and particle c. These variables are relativistic invariants.

The rapidity y and transverse momentum p_T of particle c. In the CM, the rapidity is defined by $y = \frac{1}{2}\log[(E+p_L)/(E-p_L)]$ and similarly in other reference frames. The rapidity has simple additive properties under Lorentz transformations.

The momentum p and emission angle Θ of particle c in a specified frame.

The kinematical relations between these different sets of variables are given explicitly in [8].

TABLE I

Variables and Lorentz-invariant cross-section

Variables	Invariant cross-section	Asymptotic expression $s \to \infty$	Remarks
	$\dfrac{Ed^3\sigma}{d^3p}$		
p_L, p_T	$\dfrac{E}{\pi}\dfrac{d\sigma}{dp_L dp_T^2}$		
$p_L^{(t)}$, p_T	$\dfrac{E^{(t)}}{\pi}\dfrac{d\sigma}{dp_L^{(t)} dp_T^2}$		
x, p_T	$\dfrac{2E}{\pi\sqrt{s}}\dfrac{d\sigma}{dx dp_T^2}$	$\dfrac{\lvert x\rvert}{\pi}\dfrac{d\sigma}{dx dp_T^2}$	with $x = \dfrac{2p_L}{\sqrt{s}}$
M, t	$\dfrac{2\sqrt{s}}{\pi}p_a^*\dfrac{d\sigma}{dt dM^2}$	$\dfrac{s}{\pi}\dfrac{d\sigma}{dt dM^2}$	p_a^* = CM momentum of incident particle
x, t	$\dfrac{E_a^*}{\pi}\dfrac{2}{\sqrt{s}}\dfrac{d\sigma}{dt dx}$	$\dfrac{1}{\pi}\dfrac{d\sigma}{dt dx}$	E_a^* = CM energy of incident particle
y, p_T	$\dfrac{1}{\pi}\dfrac{d\sigma}{dy dp_T^2}$		
p, Θ	$\dfrac{E}{2\pi p^2}\dfrac{d\sigma}{dp\, d(\cos\Theta)}$		

The Lorentz invariant differential cross-section, or inclusive structure function $F_1 = E_c d^3\sigma/d^3p_c$ is given in Table I as expressed with the different sets of variables. The function F_1 has the interesting property

$$\langle n_c \rangle = \frac{1}{\sigma_{in}}\int \frac{d^3\sigma}{d^3p_c}\, d^3p_c = \frac{1}{\sigma_{in}}\int \frac{1}{E_c} F_1 d^3p_c,$$

where σ_{in} is the total inelastic cross-section and $\langle n_c \rangle$ is the average multiplicity for production of particle c.

Feynman "scaling" implies that $F_1(x, p_T, s)_{s\to\infty} \to F_1(x, p)$, "Limiting fragmentation" *e. g.* of the target, that $F_1(p_L^{(t)}, p_T, s)_{s\to\infty} \to F_1(p_L^{(t)}, p_T)$. These predictions are closely related [9, 10].

Exclusive reactions where 2 particles are measured in the final state are $a+b \to c+d+X$ and the inclusive structure function of second order is defined by

$$F_2 = E_c E_d d^6\sigma/d^3p_c d^3p_d \tag{1}$$

and similarly for higher orders. Here

$$\frac{1}{\sigma_{in}} \int \frac{1}{E_c E_d} F_2 d^3p_c d^3p_d = \langle n_c(n_c-1)\rangle \quad \text{if } c = d,$$
$$= \langle n_c n_d\rangle \quad \text{if } c \neq d,$$

from which may be defined the integrated correlation parameter f_2:

$$f_2 = \frac{1}{\sigma_{in}} \int \frac{1}{E_c E_d} F_2 d^3p_c d^3p_d - \frac{1}{\sigma_{in}^2} \int \frac{1}{E_c} F_1(p_c) \frac{1}{E_d} F_1(p_d) d^3p_c d^3p_d =$$
$$= \langle n_c(n_c-1)\rangle - \langle n_c\rangle^2 \quad \text{if } c = d,$$
$$= \langle n_c n_d\rangle - \langle n_c\rangle \langle n_d\rangle \quad \text{if } c \neq d. \tag{2}$$

1.3. Plan

Excellent lecture notes [8, 11, 15, 16, 17], review articles [10, 12, 13, 14, 20] and compilations [18, 19] on inclusive reactions are published. The present lectures have the more modest aim of illustrating the subject of inclusive reactions at conventional accelerators by some typical examples and a few recent results. In Sect. 2, the average multiplicities and related quantities, directly linked to inclusive cross-sections by relations (1) and (2), are examined, particularly for positive particles. In Sect. 3, examples of the experimental properties of longitudinal spectra are taken from K^+p reactions. Sect. 4 is devoted to the detailed properties of transverse momenta.

1.4. Acknowledgements

The author is very grateful to the organizers of the school for their warm and charming hospitality. He appreciated greatly the opportunity of witnessing the stimulating atmosphere of their high energy groups. He is grateful to several of his colleagues of the CERN K^+ group, and particularly to P. Chliapnikov, B. Dunwoodie and J. Tuominiemi for help in preparing these notes. He thanks his collaborators of the Birmingham-Brussels-CERN-Mons-Paris-Saclay (BBCMPS) Collaboration for use of some of their experimental results in course of preparation, as well as D. R. O. Morrison and his colleagues of the Aachen-Berlin-Bonn-CERN-Cracow-Heidelberg-London-Vienna-Warsaw Collaboration (ABBCCHLVW).

2. Particle multiplicities

2.1. Topological cross-sections

Data showing the energy dependence of the topological cross-sections for proton proton collisions were already presented at this school; they are shown here on Fig. 1 for completeness [20]. Except for the high energy cosmic-ray points, all results are from bubble chamber experiments. Less extensive data exist for π^- (Fig. 2) and K^- (Fig. 3) incident on protons, extended to 50 and 32 GeV incoming momenta, respectively, by the Mirabelle

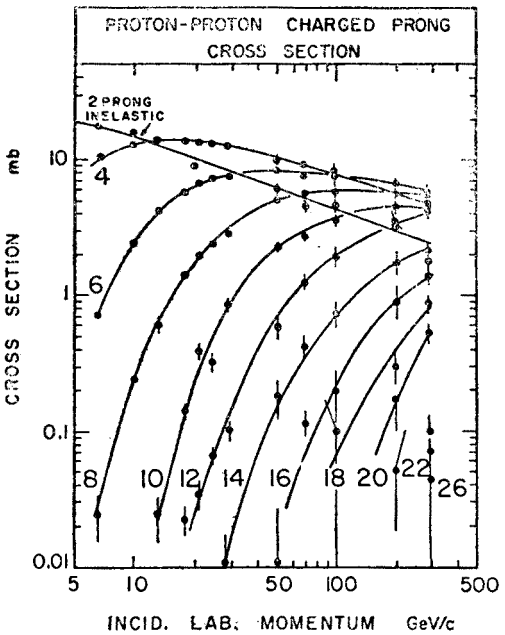

Fig. 1. Topological cross-sections for pp interactions [20]

Collaboration [21]. For incident K^+, (Fig. 4) data became available recently up to 16 GeV [22], a recent exposure of the Mirabelle bubble chamber at Serpukhov is expected to give data at 32 GeV.

A cursory examination shows that the curves are quite similar: for each topology, the cross-section appears to rise sharply from threshold, to reach a flat maximum and then to decrease slowly as the incident energy increases. More precisely, this behaviour, visible for 2, 4, 6 and perhaps 8 prongs for incident protons, can be seen unambiguously for other incident particles only for the 4-prong cross-section. The position of the maximum of the 4-prong cross-section is particle-dependent, it occurs in the neighbourhood of 20 GeV for pp, 15 GeV for K^-p and 5 GeV for π^-p.

The K^-p total cross-section is known to decrease with increasing incoming energy. This decrease is mostly due to the decreasing 2-prong inelastic cross-section. The zero-prong decreases even more sharply. The decrease of the total cross-section is usually inter-

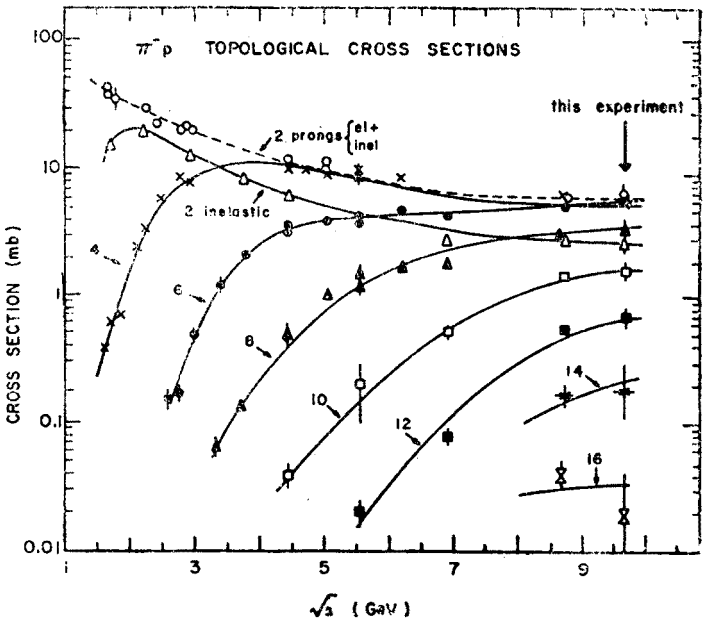

Fig. 2. Topological cross-sections for π^-p interactions [21]

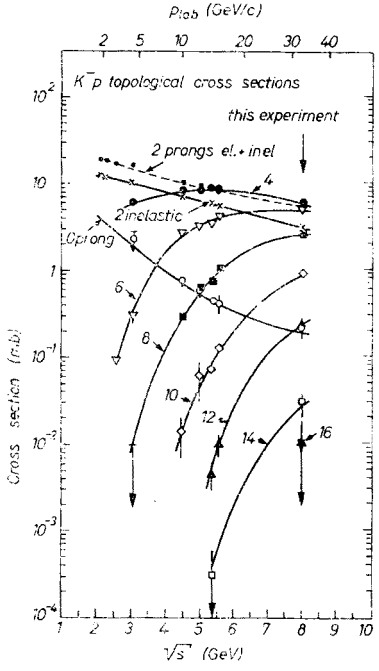

Fig. 3. Topological cross-sections for K^-p interactions [21]

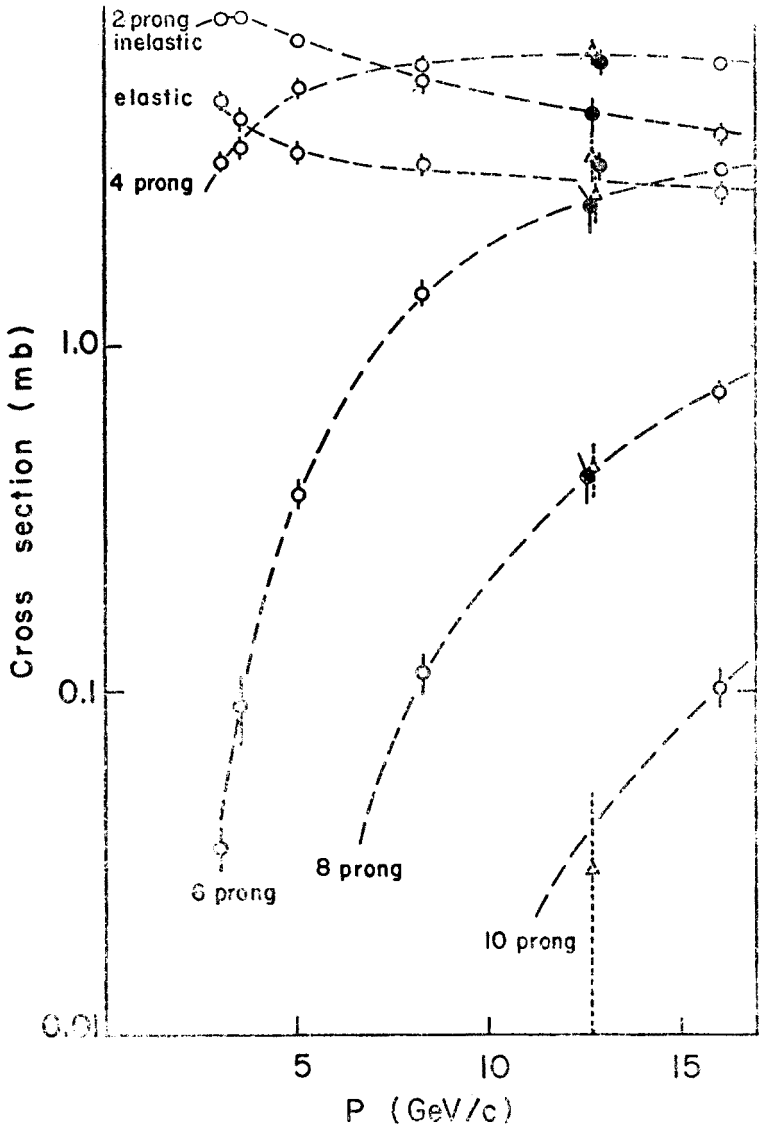

Fig. 4. Topological cross-sections for K^+p interactions [22]. The point at 12.7 GeV is indicated before (dotted) [23], and after the correction explained in the text

preted, in Regge phenomenology, by the decreasing contribution of Regge trajectories that are lower than that of the dominating Pomeron. Why this decrease is mostly linked to inelastic two-prong reactions seems to be an interesting problem.

For the π^- induced reactions, it has been noted already that the 4-prong reaches its maximum at the relatively low energy of 5 GeV. By contrast, the 6-prong cross-section is still increasing at 50 GeV, quite unlike the pp case.

Experimental remarks: the inelastic 2-prong cross-section at 12.7 GeV [23] appears anomalously low and, as will be seen below, the mean multiplicity and dispersion are not easily compatible with values at neighbouring energies. If the 2-prong cross-section is arbitrarily increased to lie on the curve, and if the other topological cross-sections at 12.7 Gev are corrected accordingly (keeping the total cross-section constant), a smooth behaviour is restored for all curves. Similarly, it may be useful to point out that the topological cross-sections of Smith *et al.* [24] for pp, are specified by the authors to be

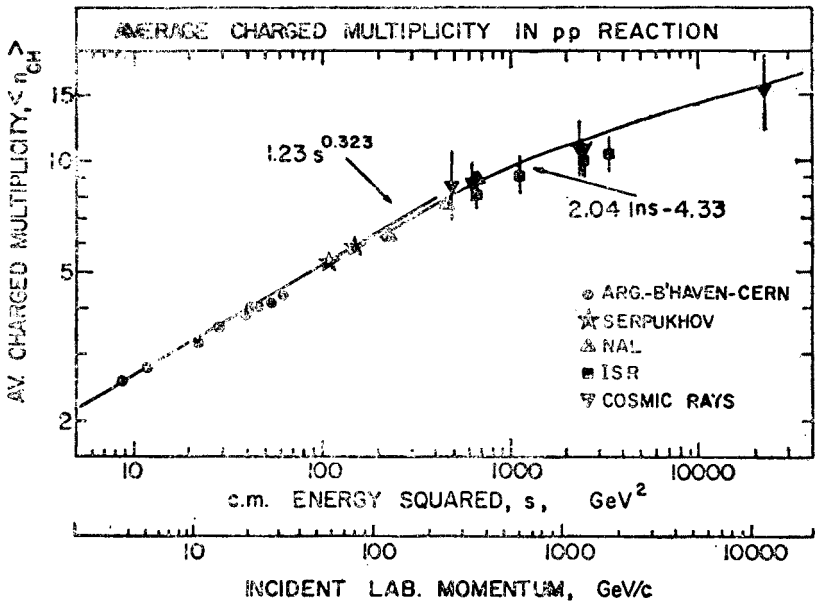

Fig. 5. Average multiplicity for pp interactions [25]. Lines are drawn to show a power law at low energy and a logarithmic dependence at high energy. A logarithmic dependence is also acceptable at low energy (see Fig. 6) but not throughout the whole range of energy (double logarithmic plot)

without the contribution of strange particle production. Yet, they are often erroneously quoted as total topological cross-sections: this mistake changes, for instance, the average multiplicity by 0.12 at 28 GeV.

2.2. Average charge multiplicity

The average number of charged particles observed in the final state, or average charge multiplicity $\langle n_{ch} \rangle$ for pp collisions is shown by Figs 5 and 6, as a function of s, the square of the total energy in the CM. There is a strong indication of upward curvature on Fig. 6, showing that a simple log s dependence is not valid over the whole range of observations. It has been attempted to fit the lower energy region by a $s^{1/3}$ dependence, and the higher energy region by log s. These descriptions are inspired by theoretical conjectures of Satz [26] and Berger & Krzywicki [27]. These authors observe that, in the low energy region, the longitudinal momentum p_L and transverse momentum p_T are of the same order of

magnitude, the phase space is thus spherical, leading to an energy dependence in $s^{1/3}$. By contrast, in the high energy region, p_T remaining limited, the phase space is cylindrical, leading to an energy dependence in $\log s$.

However, the experimental evidence is not compelling. Indeed, even in the low energy region, $E_{inc} \leqslant 50$ GeV, where data are available for π^+p, K^+p and pp reactions, a law of the form $a+b \log s$ gives very good fits [22], as shown by Fig. 6 and Table II.

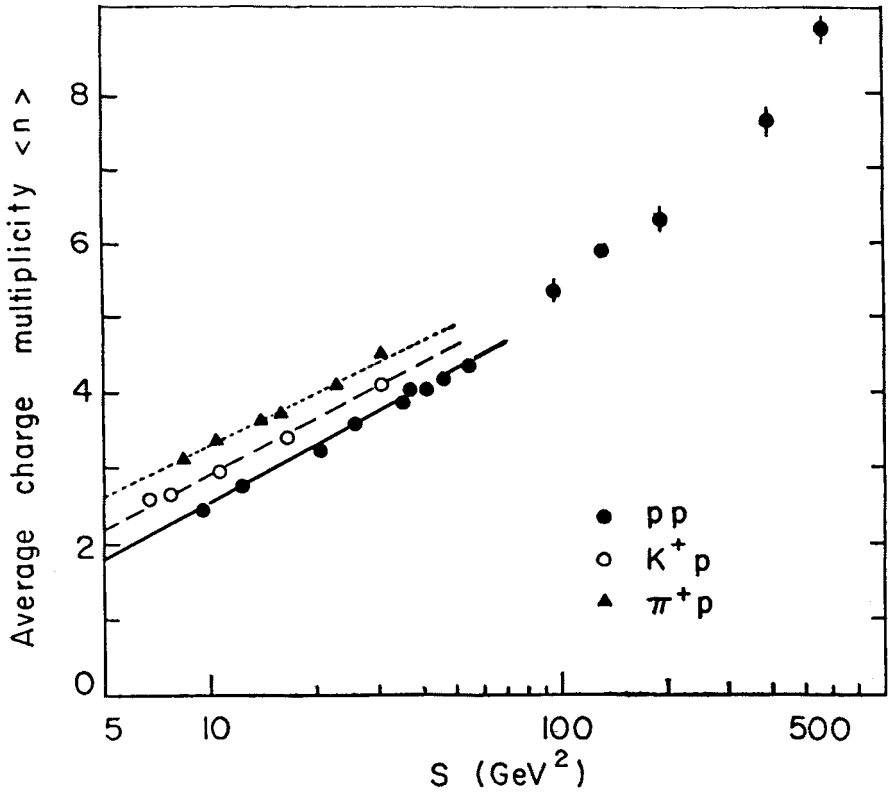

Fig. 6. Average multiplicity as function of s for π^+p, K^+p and pp interactions [22]. Lines are fits to $a+b \log s$, results are given in Table II (semi logarithmic plot)

The data show clearly that there are systematic differences between the average multiplicities induced by different incident particles. Indeed, there is a consistent tendency of the constants a to increase, and b to decrease, with decreasing mass of the incident particle: this may be expressed more quantitatively by noting that, from Table II

$$\frac{a_K - a_\pi}{a_p - a_\pi} = 0.50 \pm 0.20, \qquad \frac{b_\pi - b_K}{b_\pi - b_p} = 0.50 \pm 0.07$$

whereas

$$\frac{m_K - m_\pi}{m_p - m_\pi} = 0.443.$$

TABLE II

Fits to $\langle n \rangle = a + b \ln s$

Beam Particle	χ^2/N	b	a	p (Beam) range GeV
π^-	8.3/6	1.474 ± 0.029	-0.81 ± 0.09	6.8–50.0
K^-	13.6/2	1.384 ± 0.064	-0.77 ± 0.21	10.0–33.8
K^+	8.1/3	1.04 ± 0.02	0.52 ± 0.06	3–16
π^+	44.8/4	0.98 ± 0.02	1.04 ± 0.05	4–16
p	1.6/7	1.14 ± 0.02	-0.12 ± 0.05	4–28.4
γ		$.93 \pm .12$	1.01 ± 0.22	

Fits to $D = A\langle n \rangle + B$

Beam Particle	χ^2/N	A	B	p (Beam) range GeV
π^-	79/6	0.443 ± 0.013	-0.07 ± 0.05	6.8–50.0
K^-	6.3/2	0.454 ± 0.020	-0.04 ± 0.08	10.0–33.8
K^+	1.9/3	0.534 ± 0.011	0.454 ± 0.032	3.0–16.0
π^+	7.2/4	0.497 ± 0.014	0.405 ± 0.055	4.0–16.0
p	23/12	0.588 ± 0.007	-0.583 ± 0.027	4.0–303.0

Both the initial value a and the slope b are incident-mass dependent. The tendency appears to continue for even lower masses: the average multiplicity for photons, presented at this school by P. Söding, gives the result of the last line of Table II. However, as the square of the photon mass becomes negative (virtual photons of inelastic electroproduction) the average multiplicity appears to decrease.

It has been conjectured [29] that the multiplicity distribution, or at least the average charged multiplicity, may become independent of the incident particle, if plotted as a function of the kinetic energy Q available in the CM of the collision (total CM energy minus the masses of the incident particles). Fig. 7, as compiled by the Mirabelle collaboration [21], shows that, if indeed the data seem to follow roughly a single curve, when plotted against Q, this is only a first rough approximation. A closer examination shows, for instance, that the points for positive particles are systematically above those for the negative. Some premature enthusiasm for an "universal law of average multiplicities" should therefore be dispelled. Fig. 8 shows the data available for positive particles in more detail, systematic differences are clearly visible.

The experimental information available on the multiplicity of neutral particle production is very limited, and summarized [30] on Fig. 9. The average number of neutral pions is given as a function of the number of simultaneously produced negative particles.

It appears that, in the low energy region (19 GeV) the number of π^0's is roughly constant and independent of the number of charged particles. As the energy increases to NAL values, an approximately linear rise is observed. Several conjectures have been made to explain this behaviour [31]. These observations underline the interest to measure both the charge and the neutral multiplicities, thus obtaining the total multiplicity as function of energy.

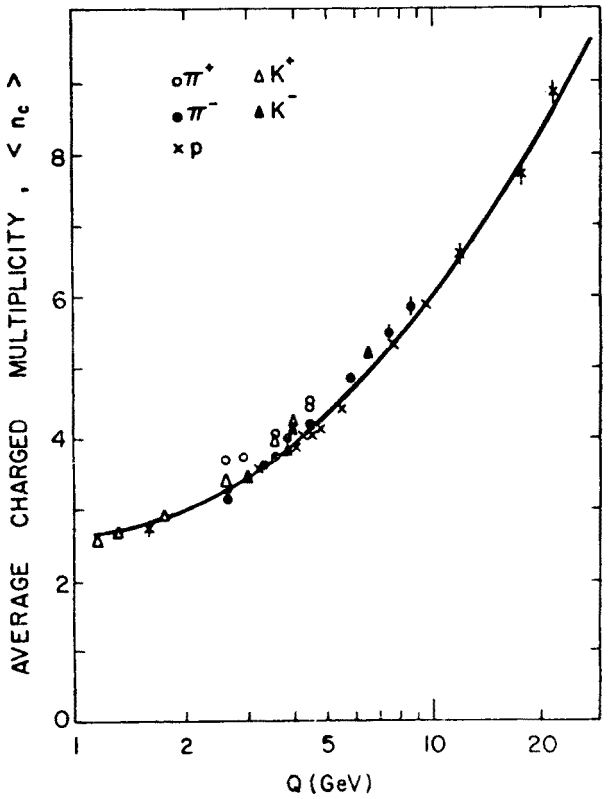

Fig. 7. Average multiplicity $\langle n \rangle$ as a function of the center of mass available energy Q (curve hand drawn) [21]

It has been argued [32] that the average multiplicity $\langle n \rangle$ may not be the most relevant quantity for comparisons with models of particle production, but that the mode or the median may provide more sensitive tests. This is illustrated by Fig. 10, and has close relations with the dispersion and with the shape of the multiplicity distributions, discussed in the following sections.

2.3. Dispersion

The dispersion of the charge distribution, $D = \sqrt{\langle n^2 \rangle - \langle n \rangle^2}$ is plotted as a function of the average multiplicity $\langle n \rangle$ on Fig. 11, as well as the integrated correlation function $f_2 = \langle n(n-1) \rangle - \langle n \rangle^2$, for incident positive particles. There are striking similarities be-

tween π^+p, K^+p and pp: in each case, D appears to vary linearly with $\langle n \rangle$, the parametrization $D = a + b\langle n \rangle$ suggested by Wróblewski [33] fits the data very well, but the coefficients a and b are incident-particle dependent. Correspondingly, the dependence of f_2 on $\langle n \rangle$ is parabolic. The differences between the different incident particles are even more striking for f_2 than for D. Indeed, the differences seem to increase as $\langle n \rangle$ and the incident

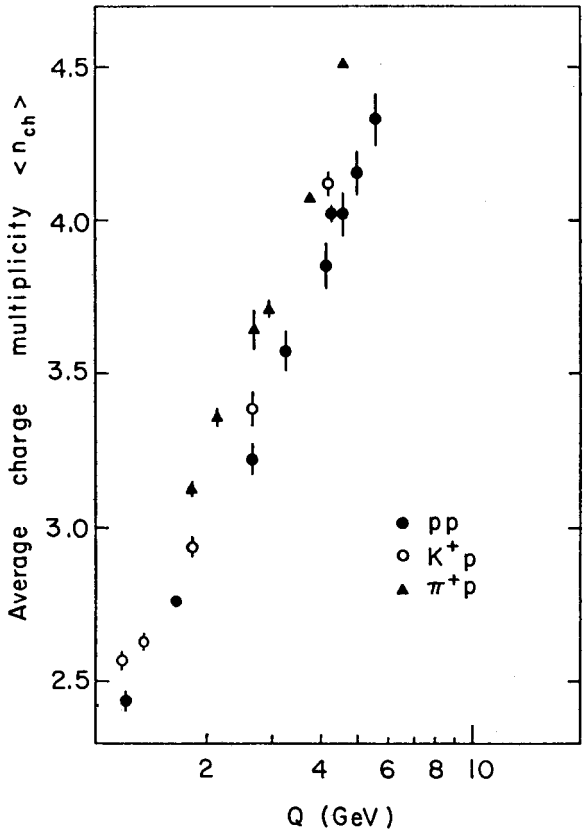

Fig. 8. Average multiplicity $\langle n \rangle$ as a function of the center of mass available energy Q (same as Fig. 9 but on an enlarged scale) for positive particles [22]. Systematic differences are seen for different incident particles

energy is raised, the lines of Fig. 11 diverge, indicating that the correlations may be quite different for different incident particles.

As the curves of D (and f_2) plotted against $\langle n \rangle$ do not coincide for the different incident particles, it is clear that D (or f_2) and $\langle n \rangle$ cannot be simultaneously functions of a single particle independent quantity, such as conjectured for the parameter Q [29, 21]. This result is demonstrated again by Fig. 12, similar to Fig. 10 but displayed on a wider energy range, where the data for negative particles are also shown. It is seen that f_2 is negative at low incident energy — a behaviour usually interpreted as due to the prevalence of correlations due to the constraints of energy and momentum conservation amongst

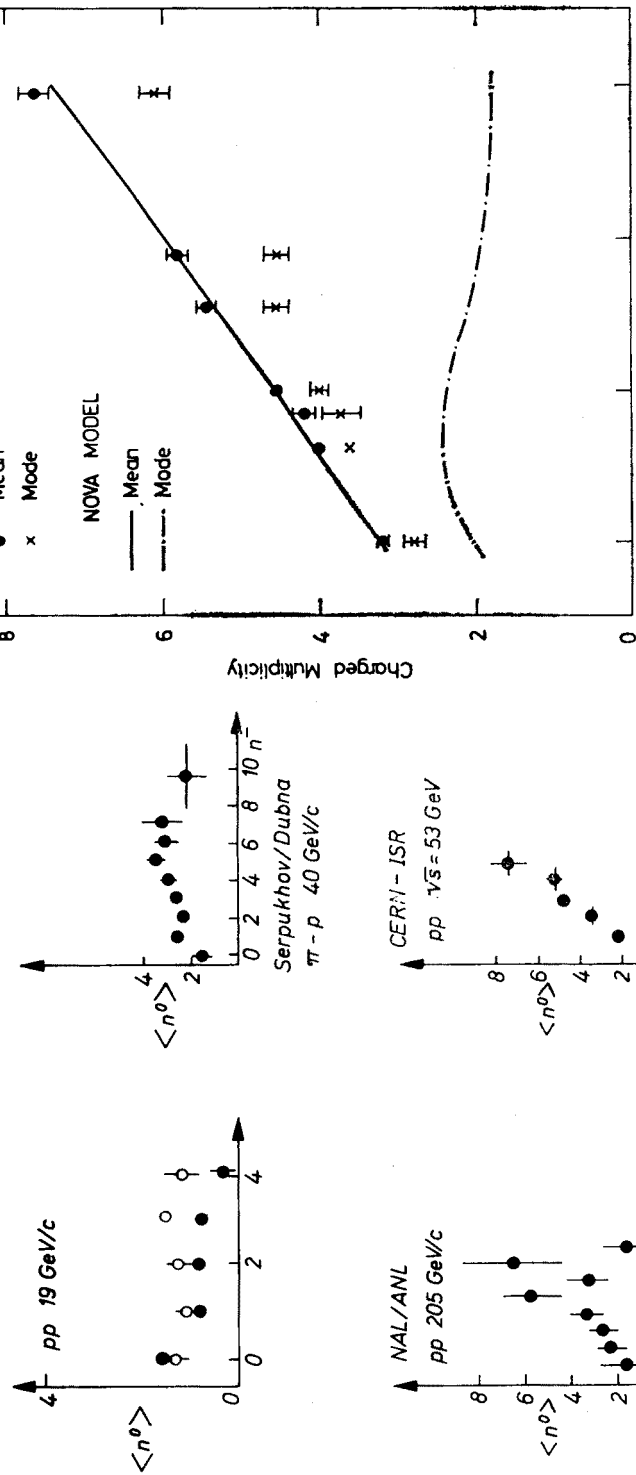

Fig. 9. Average multiplicity of neutral particles [30] as function of the average number of negative particles

Fig. 10. Mean and mode of the multiplicity distribution for pp collisions [32]. The curves are obtained from the Nova model, not discussed in the text

a small number of emitted particles — then passes through zero, around 50 GeV, and becomes positive.

Experimental remark: The need for a correction of the 12.7 GeV K^+p topological cross-sections was discussed in Sect. 2.1. On Fig. 11 the effect of the correction is shown, and restores the smoothness of the curves for D and f_2 *vs* $\langle n \rangle$.

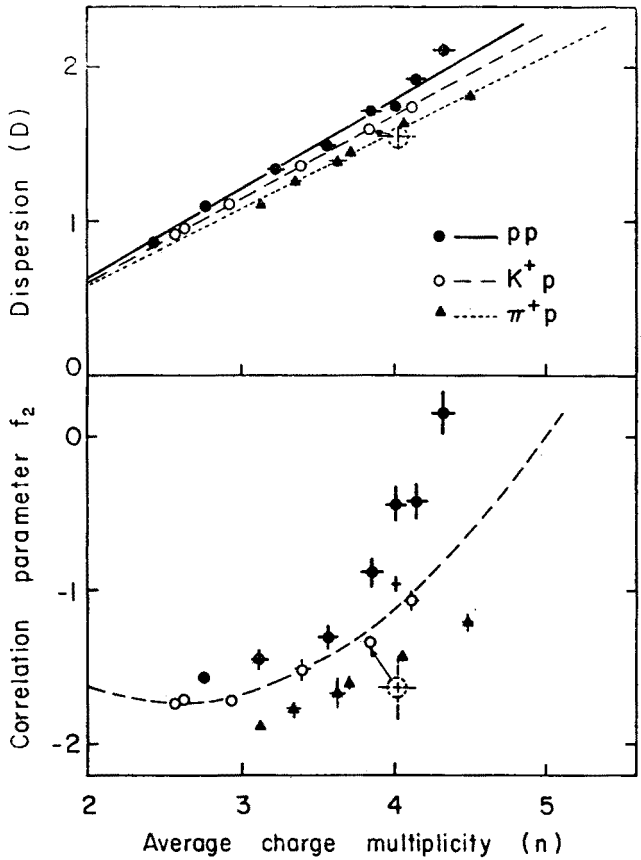

Fig. 11. Dispersion D and integrated correlation parameter f_2 as functions of the average multiplicity $\langle n \rangle$ [22], for positive particles. The point at 12.7 GeV is shown before (dotted) and after the correction explained in the text

Although a linear dependence of D on $\langle n \rangle$ seems to describe adequately the data, it is also interesting to examine the ratio $D/\langle n \rangle$, shown by Fig. 13. For pp collisions, the semi-inclusive scaling of Koba, Nielsen and Olesen [34] predicts that this ratio should become asymptotically equal to 2, well compatible with the data. The ratio $\langle n \rangle / D$ for K^- and π^- shows a somewhat stronger energy dependence and does not seem to have reached an asymptotic limit at the presently available energies.

Annihilation events [35] show a particularly interesting qualitatively different behaviour of f_2, shown by Fig. 14. The correlation function seems to be much more negative, at corresponding multiplicity than for the other reactions.

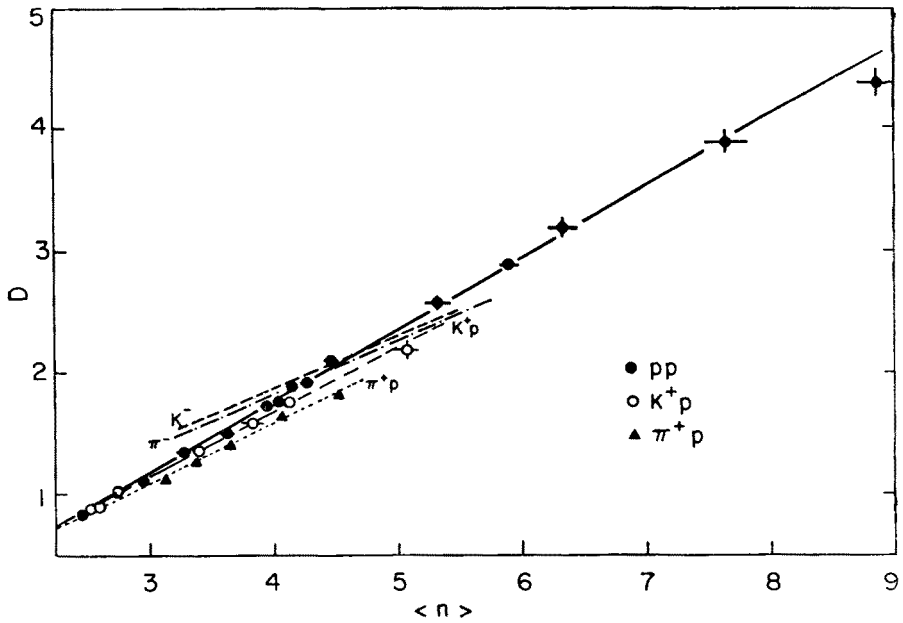

Fig. 12. Dispersion D as function of the average multiplicity $\langle n \rangle$ for positive and negative particles [22]

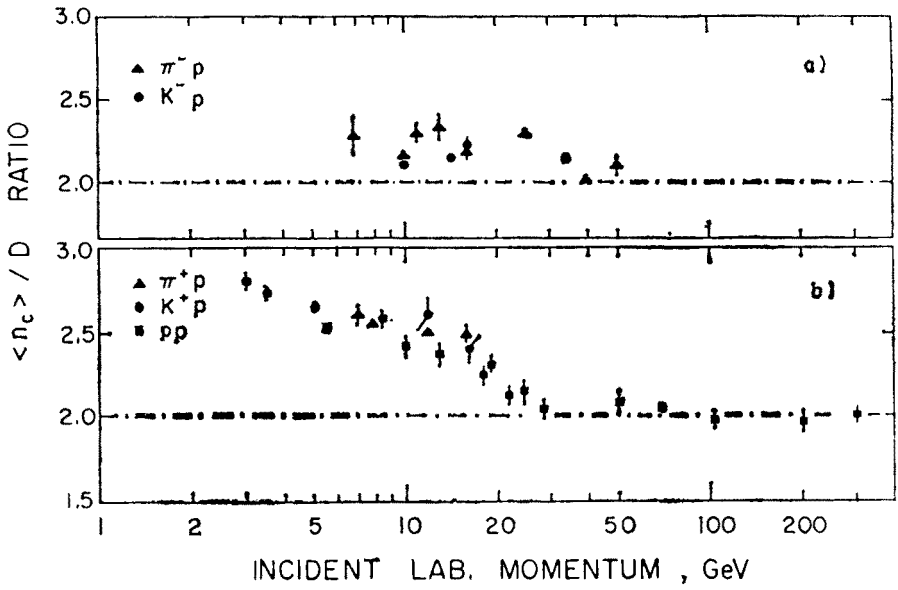

Fig. 13. The ratio $\langle n \rangle / D$ for π^-p, K^-p and π^+p, K^+p and pp collisions

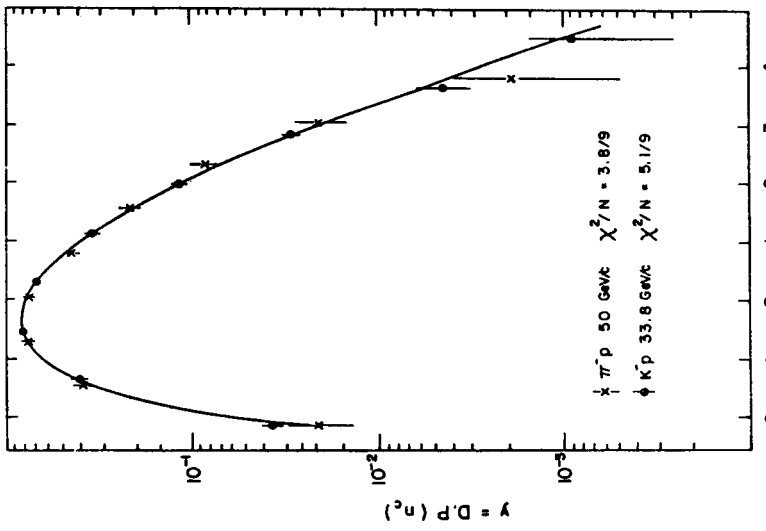

Fig. 15. An example of multiplicity distribution, for π^-p and K^-p events [21] compared to the Czyżewski-Rybicki formula

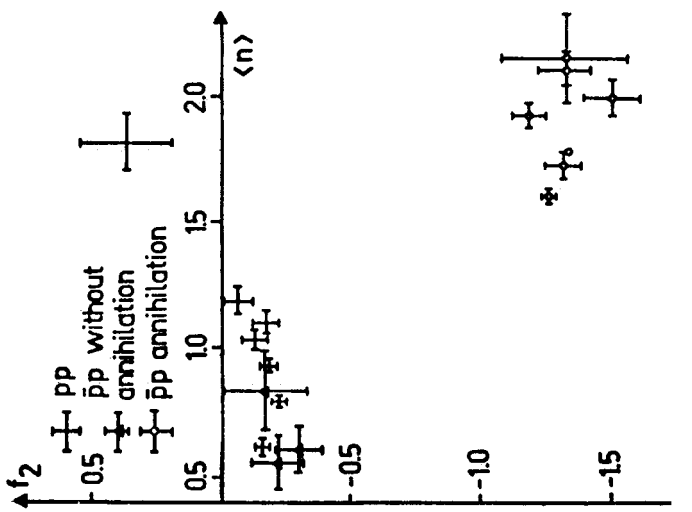

Fig. 14. The integrated correlation parameter f_2 for $\bar{p}$p interactions, showing separately the annihilation and non-annihilation events [35]

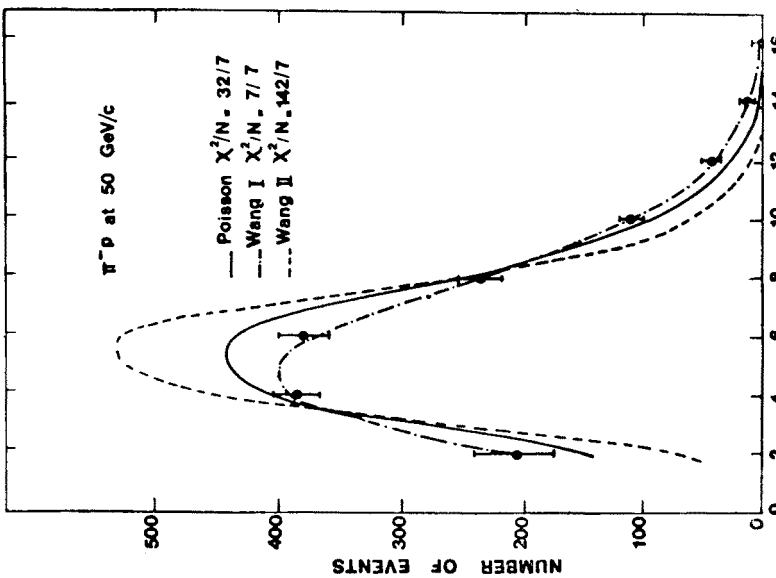

Fig. 16. Comparison of the multiplicity distribution for π^-p at 50 GeV [21] with the Poisson and Wang distributions

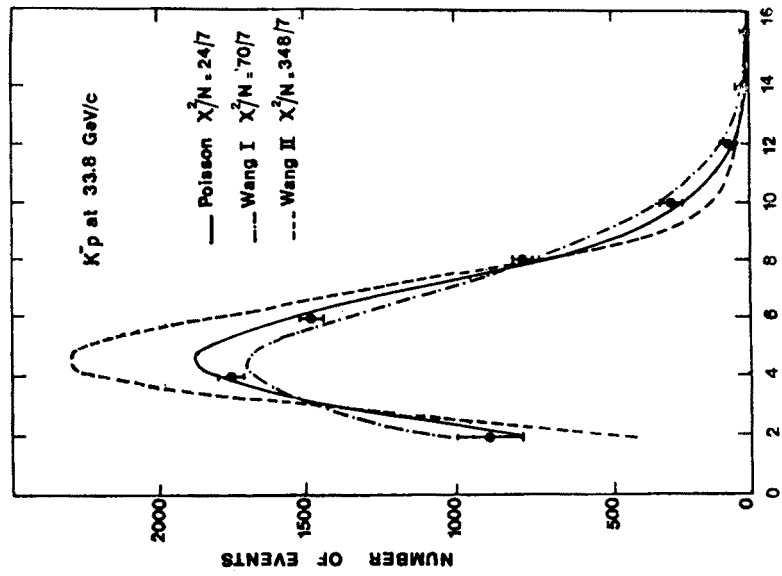

Fig. 17. Comparison of the multiplicity distribution for K^-p at 33.8 GeV [21] with the Poisson and Wang distributions

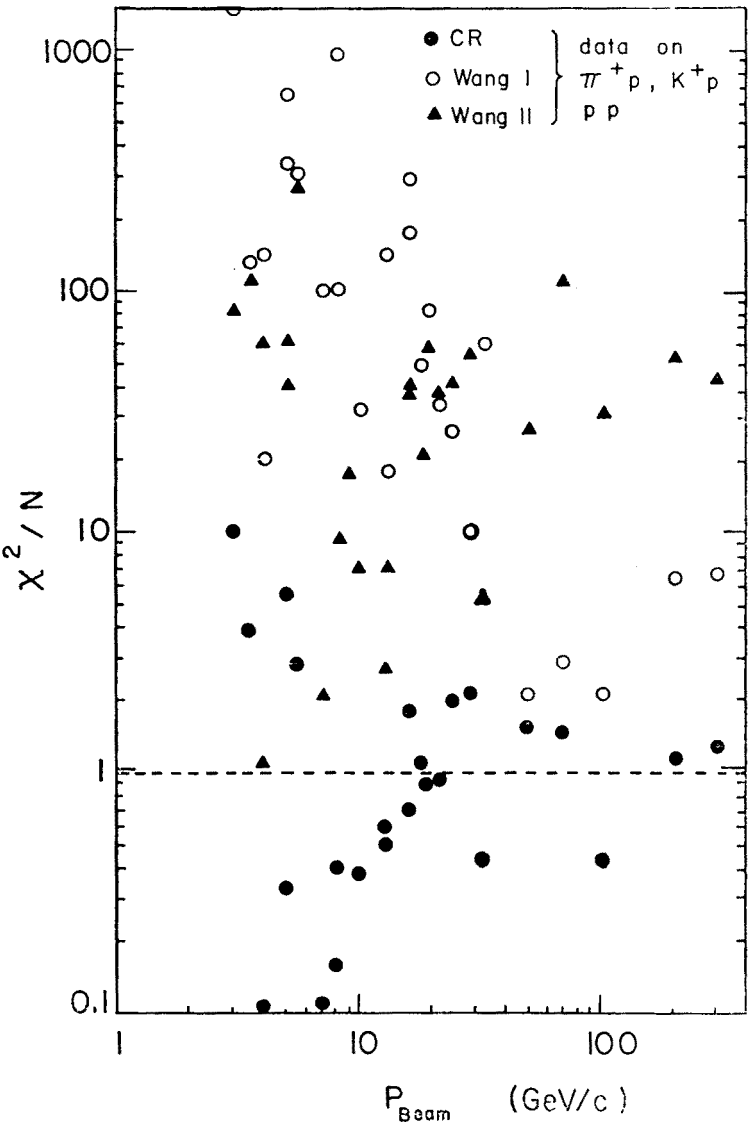

Fig. 18. Values of χ^2/N for fits of the distributions of Wang and Czyżewski-Rybicki, for positive particles at several incident energies [22]

2.4. Shape of the multiplicity distribution

The shape of the multiplicity distribution is well represented by a parametrization due to Czyżewski and Rybicki [36]. With $x = (n - \langle n \rangle)/D$ and $y = D\sigma_n/\sigma_T$

$$y = \frac{2de^{-d^2}d^{2x}}{\Gamma(1+x)}. \tag{3}$$

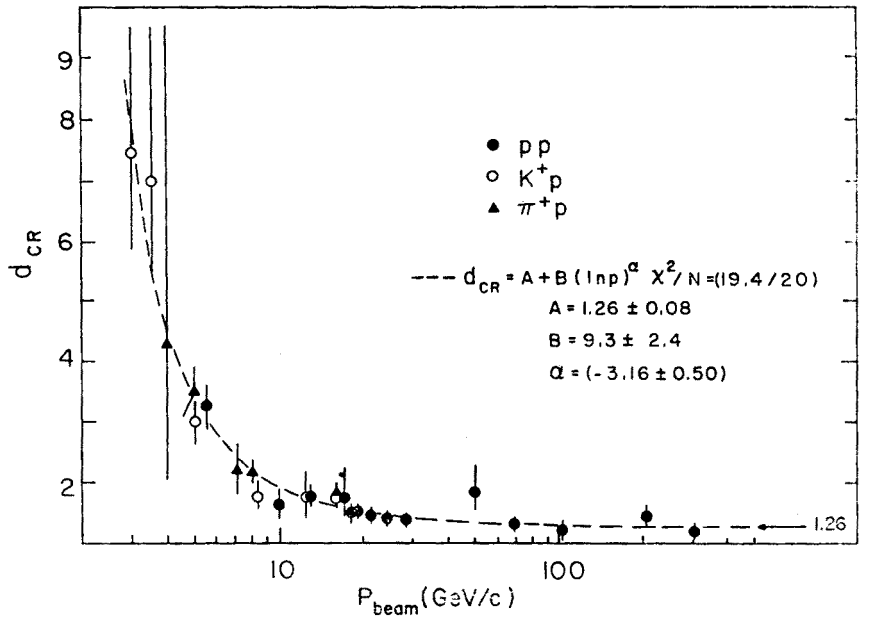

Fig. 19. Value of the parameter d_{CR} of the Czyżewski-Rybicki formula, for positive particles, as function of the incident momentum [22]. An empirical parametrization is indicated

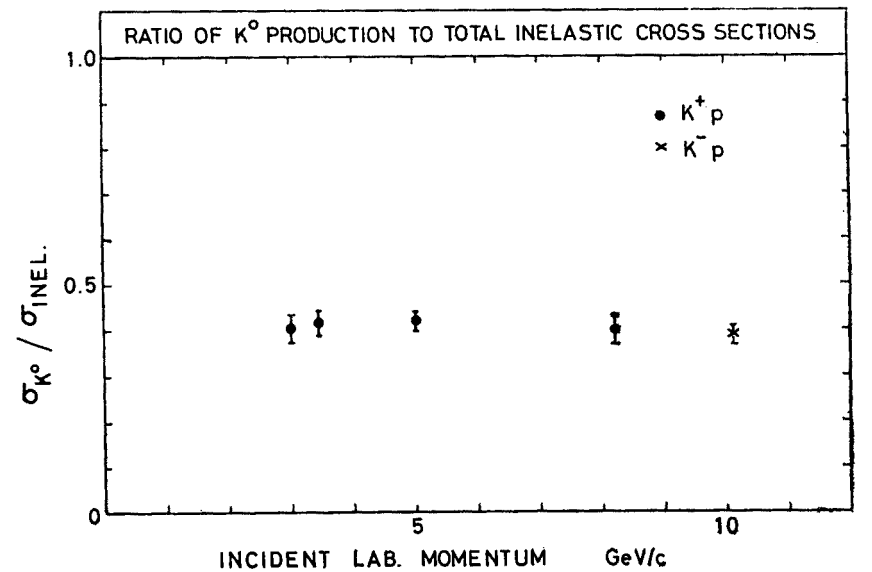

Fig. 20. Ratio of the cross-section for K^0 production to the total inelastic cross-section, for K^+p a nd K^-p, as function of incident momentum [38]

The value $d = 1.8$ was initially found by these authors, using data from $\pi^{\pm}$p and pp experiments between 4 and 28 GeV. With this value of d, the distribution (3) fits all available data reasonably well. An example is given by Fig. 15. If, in addition, and as discussed in the previous section, the ratio $\langle n \rangle / D$ is constant, then the multiplicity distribution becomes a function of $n/\langle n \rangle$ only, as predicted by Koba, Nielsen and Olesen [34]. By contrast, the data does not follow a simple Poisson distribution, nor does it agree well with the two descriptions given by Wang [37]. Examples are given by Figs 16 and 17 which show recent results [21] of the Mirabelle Collaboration.

These comments are presented quantitatively by Fig. 18, which shows the χ^2/N ratio as a function of incident momentum, for fits of the positive particle data to the distributions of Wang and Czyżewski-Rybicki, for which the fitted value of the parameter d is given by Fig. 19. It is clear that the χ^2/N values are always too high for Wang II, they may become acceptable for Wang around 50 GeV/c (where $f_2 \approx 0$) as mentioned already. The Czyżewski-Rybicki distribution always gives good fits, with an interesting tendency of d to be relatively high (4 or more) at low beam momentum, and to go down asymptotically to the value $d = 1.26$ as the energy increases.

3. Longitudinal momenta in the reactions $K^+p \to K^0 + X$, $K^+p \to K^{*+} + X$, $K^+p \to \pi^+ + X$

3.1. The reaction $K^+p \to K^0 + X$ [38]

The charge exchange inclusive reaction[1]

$$K^+p \to K^0 + X \tag{4}$$

represents a relatively large fraction of the total inelastic K^+p cross-section, as shown by Fig. 20 (a point relative to the reaction $K^-p \to K^0 + X$ is also shown, with similar behaviour). This fraction appears to vary but little for incident momentum.

The structure function F integrated over all p_T, is shown by Fig. 21 as a function of $x = p_L/p_{L\,max}$, for several incident momenta. The behaviour, quite typical of reactions in this energy region, shows several interesting features. There is a forward-backward asymmetry, with a higher forward cross-section, sometimes called leading particle effect[2], noticed whenever the observed particle has quantum numbers equal, or closely related, to those of the incident particle. For $x \sim 1$, a peak appears at low incident momentum, which is related to resonance production, mostly to the exclusive cross-section $K^+p \to K^0\Delta^{++}$ (1236), known to have a relatively high cross-section [39]. In the region roughly defined by $0.2 < x < 0.7$, a definite energy dependence is seen, its interpretation is mentioned in Sect. 3.2. For $x < 0.2$, in the central and backward regions, there is a strong indication that scaling (independence of incident energy) may be reached; the curves for 8, 12.7 and 16 GeV are quite close to each other, the last two practically coincide. Indeed, the scaling

[1] It can be shown, by an estimation of the $K\bar{K}$ production cross-section, that the data contain $\leqslant 5\%$ of $\bar{K}^0$.

[2] It has been suggested [51] to use the term "favoured particle effect" instead of "leading particle effect". The new term seems indeed more appropriate, in particular when the quantum numbers are not equal.

in the central region may even be valid separately for different values of n in each of the reactions $K^+p \to K^0 + n_{\text{charged}} + X$ *i. e.* the semi-inclusive scaling of Koba *et al.* [34]. The data are shown by Fig. 22.

The behaviour of F_1 in the region $x < 0$, which corresponds to target fragmentation, is presented as a function of laboratory longitudinal momentum $p_L^{(t)}$ in Fig. 23. The "early" scaling is seen again. In the framework of the Mueller-Regge analysis, and of the

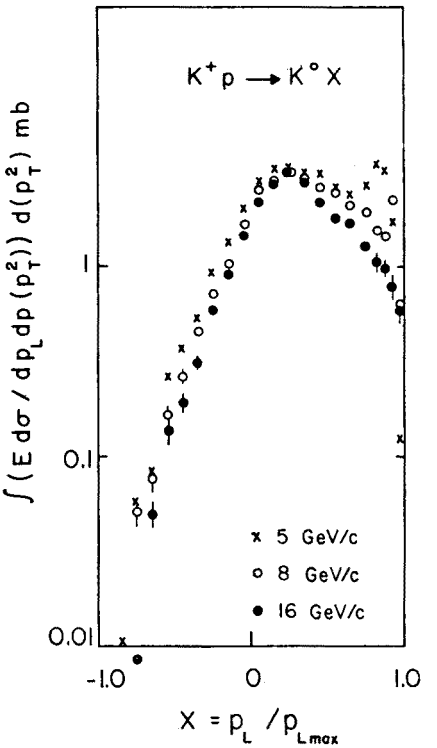

Fig. 21. Invariant cross-section $\int \frac{E}{p_{L\,\max}} \frac{d\sigma}{dp_T^2 dx} dp_T^2$ as function of x for K^+p reactions at several incident energies [22]

resulting criteria of Chan *et al.* [4] for early limiting fragmentation one may note at first sight that the incident Mueller channel *abc*, (Fig. 24a), with $a = K^+$, $b = p$, $\bar{c} = \bar{K}^0$, is non-exotic, as well as the target system $b\bar{c}$. Thus no early scaling is expected. However, as remarked by Miettinen [40] the hypothesis of factorization, or an examination of the quark diagram of Fig. 24b show that the only Regge trajectory which may be exchanged between the K^+ and the $(p\bar{K}^0)$ system, besides the Pomeron, in the trajectory of the Φ, which has a low intercept $\alpha(0)$ on the Chew-Frautschi plot. The scaling may thus be approached rapidly by a law of the form $A + Bs^{-1}$, as opposed to the more usual and slower $A + Bs^{-\frac{1}{2}}$ [3].

[3] The author is grateful to H. Miettinen, for calling his attention to this point at the School.

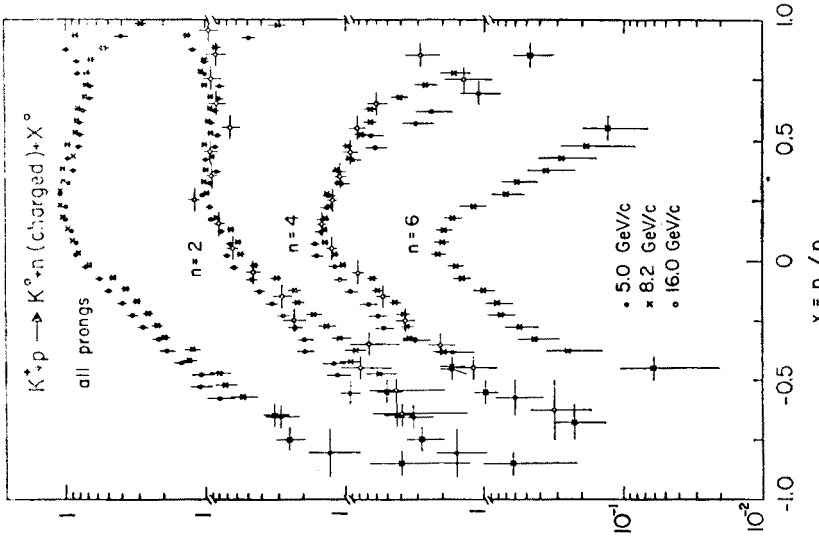

Fig. 22. Normalized invariant cross-section $\int \frac{1}{\sigma_n} \frac{D\sigma_n}{dp_L dp_T^2} dp_T^2$ as function of x for semi-inclusive K^+p reactions [38]. (The 16 GeV data for $x \sim 1$ are preliminary, and may be slightly underestimated (loss of fast K^0's)

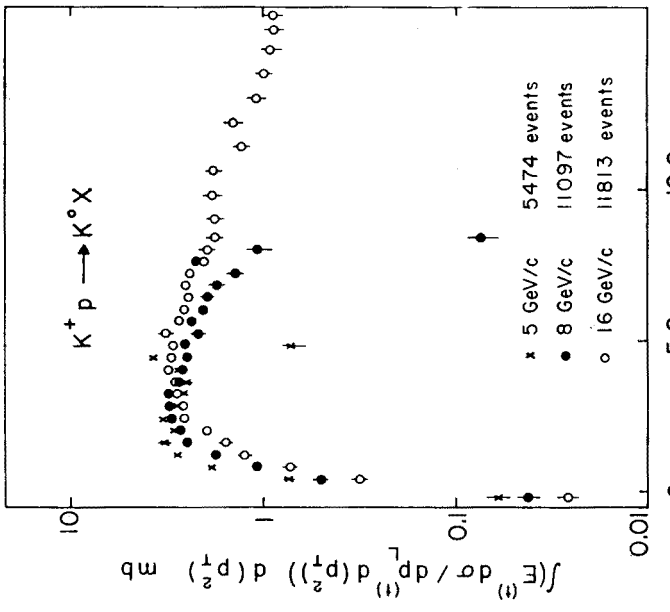

Fig. 23. Invariant cross-section $\frac{Ed\sigma}{dp_L^{(1)} dp_T^2} dp_T^2$ as function of $p_{Lab} = p_L^{(1)}$ for K^+p reactions (BBCMPS Collaboration) (same remark as for Fig. 22)

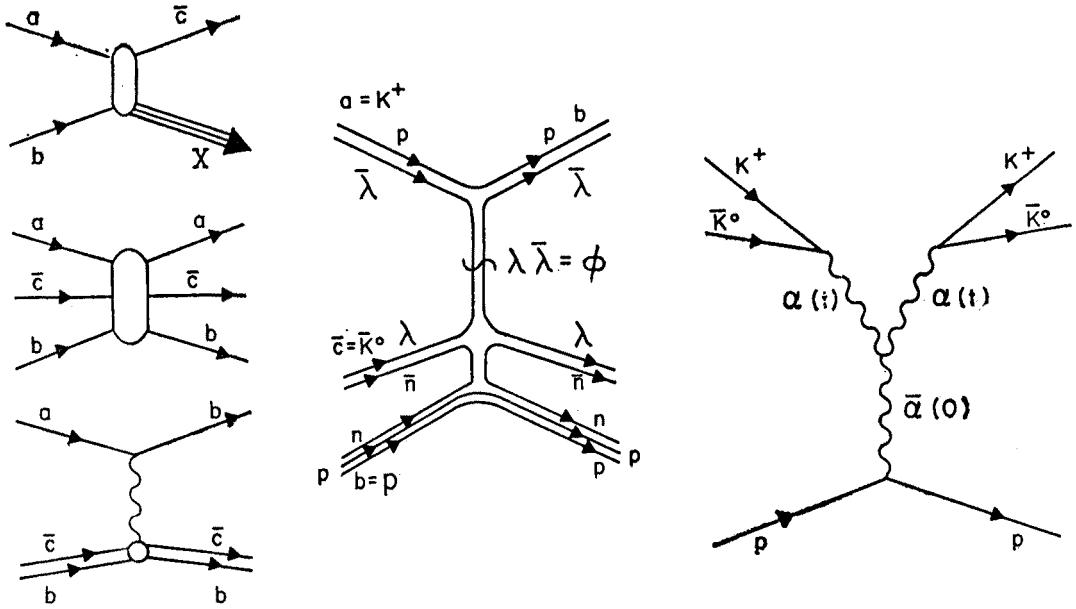

Fig. 24. Mueller-Regge diagrams. a) Illustrates the relation between the inclusive reaction $a+b \to c+X$ and the discontinuity of the three-body elastic scattering amplitude $a+b+\bar{c} \to a+b+\bar{c}$, and shows the diagram for the fragmentation of the $b\bar{c}$ system by incident a. b) Quark lines (p, n, λ) for the fragmentation of the proton into K^0, by incident K^+. It is seen that the exchanged quantum numbers between the K^+ and the target system ($p\bar{K}^0$) are those of the Φ. c) Triple Regge diagram for the amplitude ($K^+\bar{K}^0p$), corresponding to the inclusive reaction $K^+p \to K^0X$

It is interesting to note that the spectrum of the mass M of the system X recoiling against the K^0 has an exponential behaviour, as illustrated by Fig. 25. This observation leads to the Triple-Regge analysis discussed in the next Section.

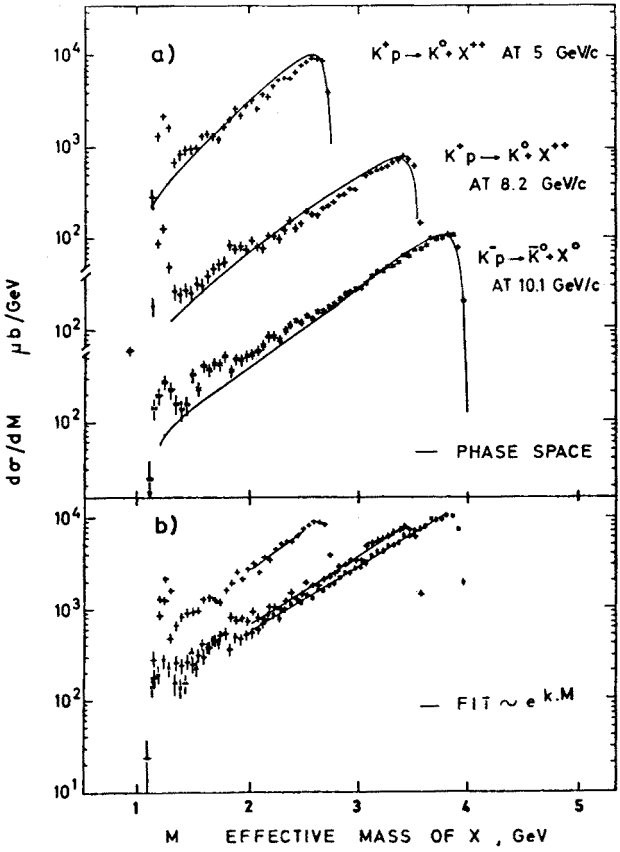

Fig. 25. Missing mass spectra for the reaction $K^+p \to K^0X$ [38] and $K^-p \to K^0X$. The "phase space" curves are computed by evaluating separately the contributions of each of the observed multiplicities

3.2. Triple Regge analysis

As shown by Chliapnikov *et al.* [41], the behaviour of the reaction may be understood in part by the triple Regge diagram of Fig. 24c expected to be valid for both s/M^2 and M large. These requirements are hardly obeyed by the available data, nevertheless the analysis is applied to the region $2 < s/M^2 < 5$, 1 GeV $< M <$ 2.2 GeV, and small $|t|$, thus $|x| > 0$. The invariant cross-section may be written as

$$E\frac{d^3\sigma}{d^3p} = \frac{d\sigma}{dtd\left(\frac{M^2}{s}\right)} \cong B(t)\left(\frac{s}{M^2}\right)^{2\alpha(t)}\frac{1}{s}M^{2\bar{\alpha}(0)},$$

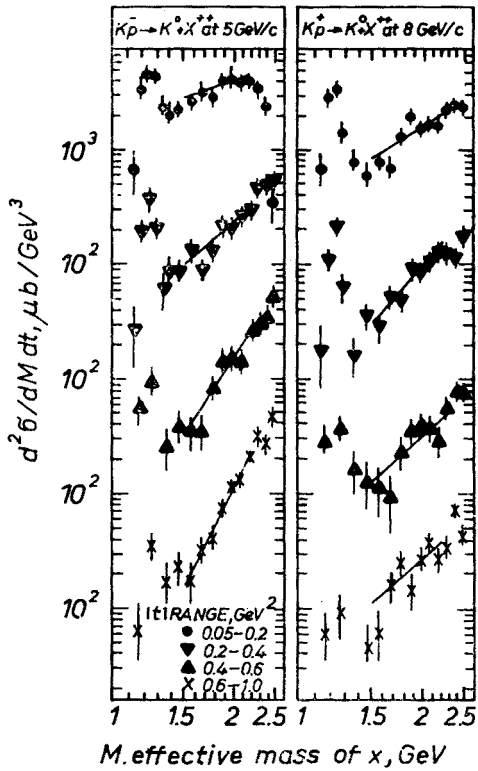

Fig. 26. Missing mass spectra for the reactions $K^+p \to K^0X$, in several intervals of t, for small $|t|$. The lines are those of the Triple-Regge model discussed in the text and illustrated by Fig. 24

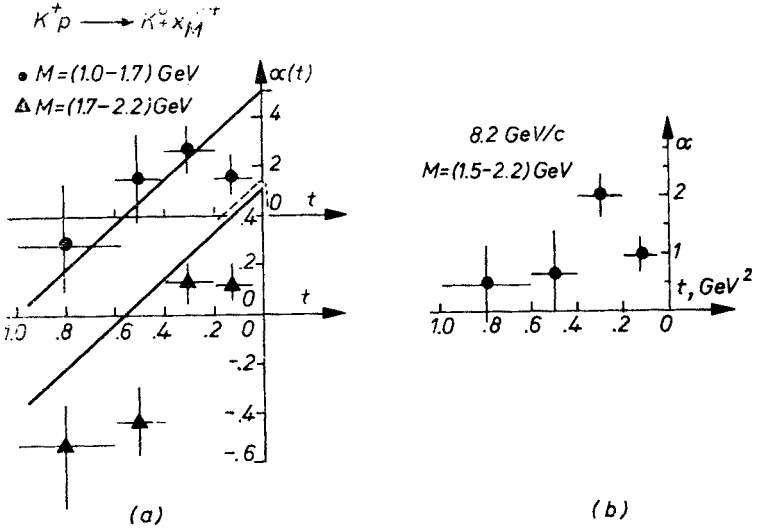

Fig. 27. a) Effective Regge trajectory $\alpha(t)$ obtained by the triple-Regge analysis [41] of the reaction $K^+p \to K^0X$, illustrated by Fig. 24 and 26, for two regions of $M(X)$. b) Intercept $\bar{\alpha}(0)$ of the effective trajectory of the Pomeron from the same analysis

where $B(t)$ contains the t dependence of the Regge residues, $\alpha(t)$ is the trajectory of the effective Regge trajectory linked to the $K^+\bar{K}^0$ vertex (ϱ, A_2 *etc.*), and $\bar{\alpha}(0)$ is the intercept of the effective Pomeron trajectory coupled to the pp vertex (Fig. 24c). Remembering that $s/M^2 \cong 1-|x|$, it is seen that the factor $(s/M^2)^{2\alpha(t)}$ obeys scaling, whereas departures from scaling occur if $\bar{\alpha}(0) \neq 1$. The exponential behaviour of the M spectrum is shown again by Fig. 26, in several regions of t, and for 2 values of the incident momentum. The resulting effective Regge trajectory $\alpha(t)$ is given by Fig. 27a for two regions of M, and the Pomeron intercept $\bar{\alpha}(0)$ is displayed on Fig. 27b for several regions of t. It is seen that

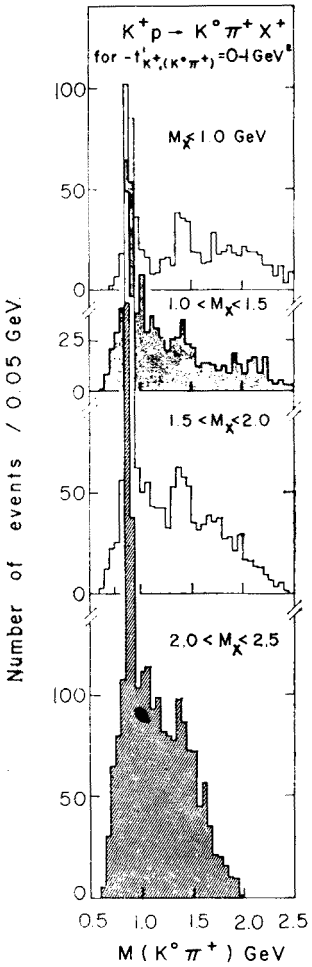

Fig. 28

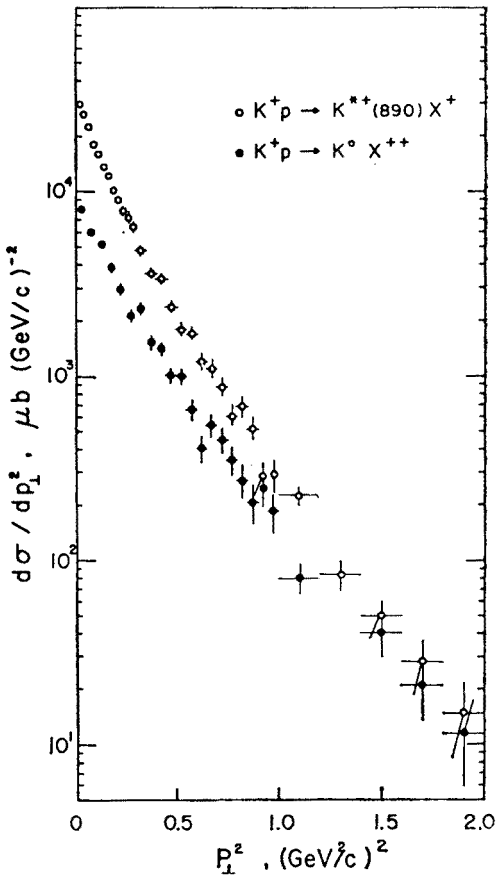

Fig. 29

Fig. 28. Effective mass spectra [42] of the reaction $K^+p \to K^0\pi^+X$, showing for different regions of $t' = |t-t_{min}|$, the production of K^* (892). The K^* are selected for further analysis of the reaction $K^+p \to K^*X$, by a cut $0.85 \leqslant K^* \leqslant 0.93$ GeV

Fig. 29. Transverse momentum squared distributions [42] of the inclusive reactions $K^+p \to K^0X$ and $K^+p \to K^*X$

$\alpha(t)$ follows roughly the expected ϱ trajectory although the experimental values tend to be too high for $1. < M < 1.7$ GeV and much too low for $1.7 < M < 2.2$ GeV. The values of $\tilde{\alpha}$ tend to depart from 1 for $t \neq 0$, as expected since the data, when integrated over all t (or all p_T) does not scale for $|x| > 0$ (Sect. 3.1).

One may conclude that the triple Regge formula gives a good qualitative description of several important properties of the reaction. Data of more statistical accuracy and

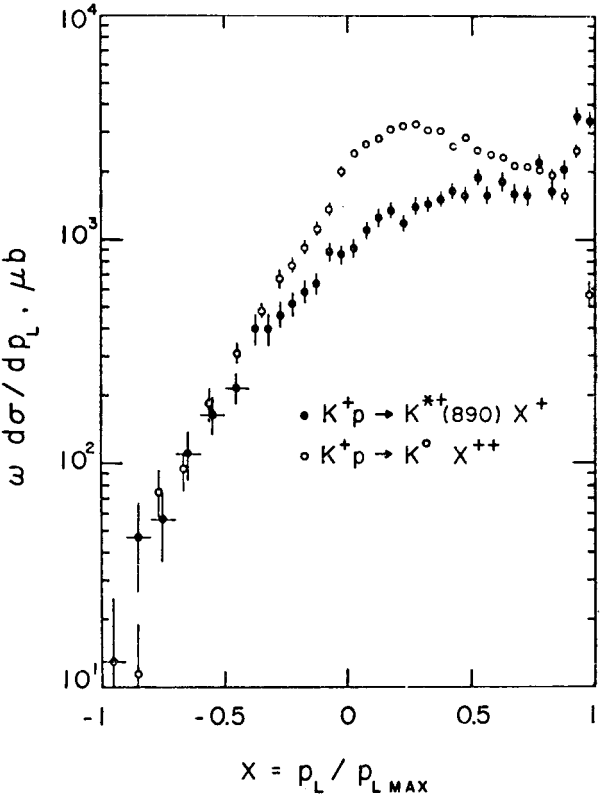

Fig. 30. Inclusive cross-section for the reactions $K^+p \to K^0p$ and $K^+p \to K^*p$ as function of $x = p_{Lmax}$

extending over a wider energy range as well as detailed comparisons with other reactions are clearly needed to establish the limits of validity of the analysis.

3.3. The reaction $K^+p \to K^*+X$ [42]

The production of $K^*(892)$ in the reaction

$$K^+p \to K^*X \tag{5}$$

is detected by the decay mode $K^* \to K^0\pi^+$, thus part of the K^0's studied in 3.1–3.2 arise from K^* decay. Some limited aspects of the contribution that the K^0, arising from K^* decay, may make to the total K^0 distribution, are examined in Sect. 3.5. Here, the K^*

signal is shown by Fig. 28, showing, for $|t_{K^+,(K^0\pi^+)}| < 1$ GeV^2, the (K^0S^+) mass spectrum for several regions of M_x. As the K^* is a relatively narrow resonance, a selection of K^* events by a mass cut $0.85 \leqslant K^*(892) \leqslant 0.93$ GeV is adequate and no background subtraction is attempted.

The distributions of transverse momenta of the K^0 in reaction (4) and of the K^* in reaction (5), are shown on Fig. 29. The two distributions are very similar, showing that

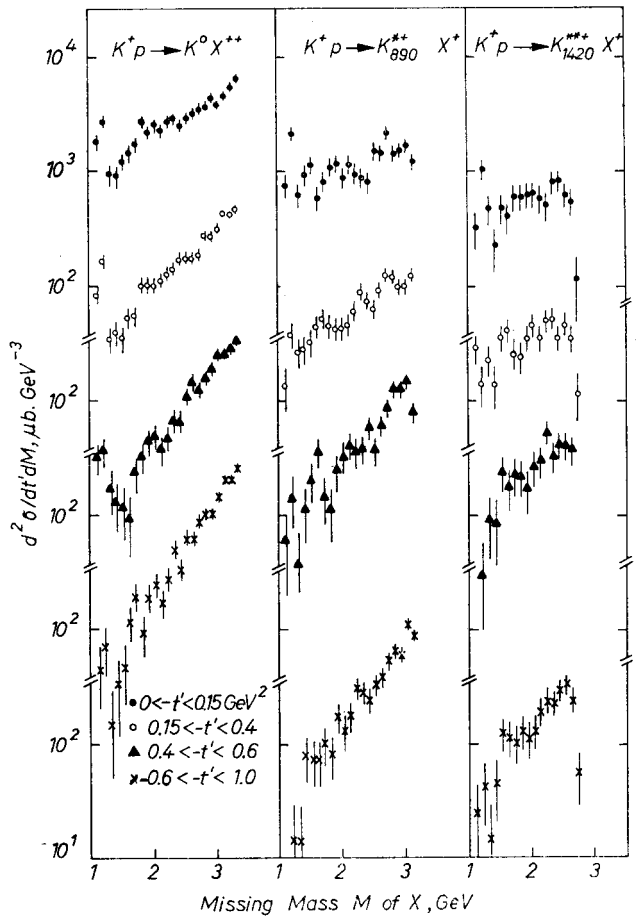

Fig. 31. $d^2\sigma/dt'dM$ distributions for the inclusive reactions $K^+p \to K^0X$, $K^+p \to K^*X$ as function of the missing mass M for several t' intervals

inclusive resonance production has features quite similar to those of particle production. This general comment is also valid for Fig. 30 which compares the x-distributions and for the exponential character of the M_x spectra, Fig. 31. Again, the $x = 1$ region shows the influence of some important exclusive reactions, including double resonance production ($K^+p \to K^*p$, $K^0p \to K^*\Delta^{++}$). The x spectrum is flatter in the forward region ($x > 0$), thus some leading particle effect remains even for the K^* production.

However, the K^* has spin 1, its alignment may be detected by the angular distribution of decay. What can be learned about spin effects in an inclusive reaction? Fig. 32 shows the behaviour of the decay angular distribution in the K^* Jackson frame, for successive regions of M. Drastic changes occur as M increases, they are also apparent on Fig. 33 which gives the spin space matrix elements of the K^* decay.

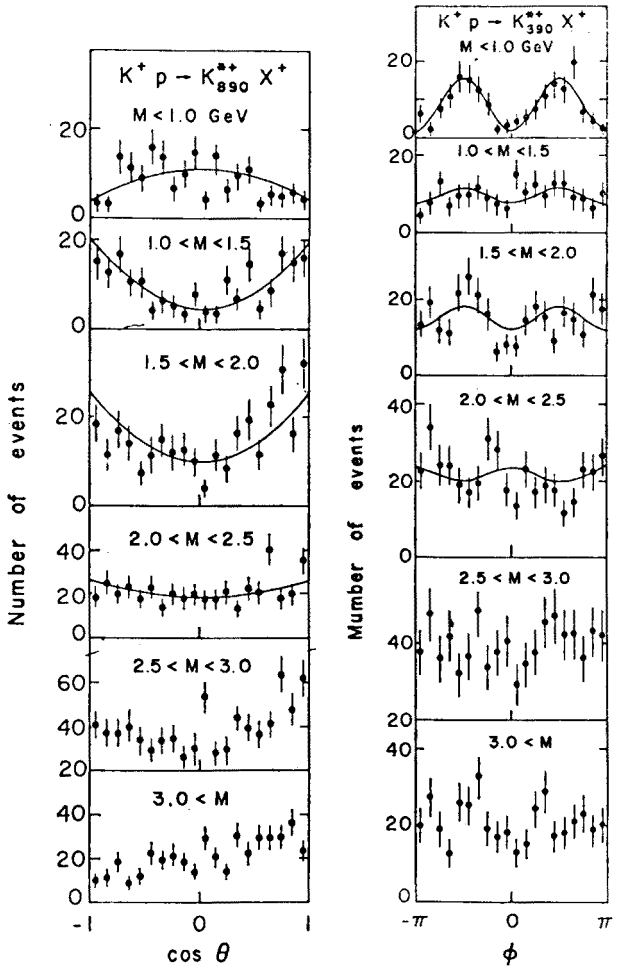

Fig. 32. Angular distribution (Jackson angles Θ and Φ) for the K^* decay in the inclusive reaction $K^+p \to K^*p$, for several regions of M

For $M < 1$ GeV, the polar angle distribution in $\sin^2 \Theta$ and the strong azimuthal anisotropy ($\varrho_{00} \simeq 0$, ϱ_{11} large) are characteristic of vector exchange, well known to dominate the prevalent $K^+p \to K^*p$ reaction [43]. For $1.0 < M < 1.5$ GeV, the distribution becomes $\sim \cos^2 \Theta$ with almost isotropic azimuthal angle (ϱ_{00} large, $\varrho_{11} \simeq 0$) again well known properties of unnatural parity exchange in the important exclusive reaction $K^+p \to K^*\Delta^{++}$ occurring in this region [44]. For higher values of M, both angular distri-

butions tend to become isotropic, showing that both exchanges with natural and unnatural parities contribute to the inclusive reaction.

One may conclude that a simple exchange model cannot be expected to describe the data. Recent investigations of two-body reactions have shown [45] that each of the Reggeized amplitudes contributing to the reactions seem to have specific t-behaviour, different from the others in important details. Similarly refined analysis of inclusive reactions will have to wait for data of much higher statistical accuracy.

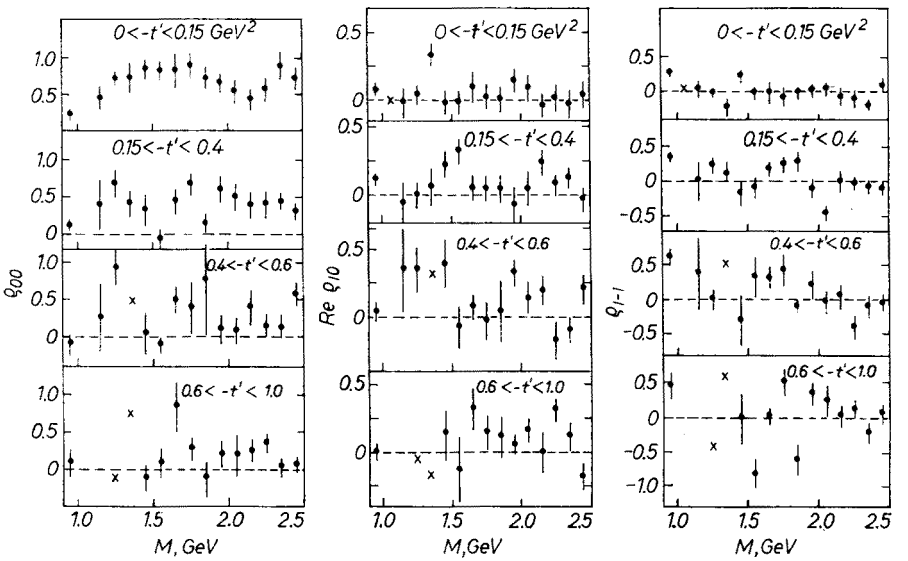

Fig. 33. Spin space density matrix elements corresponding to Fig. 32

3.4. Quark model for the reaction $K^+p \to K^0 + \pi^+ + X$

Several recent studies [46] have shown that the longitudinal spectra of inclusive reactions with incident pions or kaons become forward-backward symmetric, if trans-

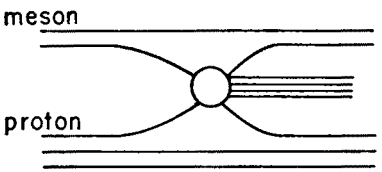

Fig. 34. Quark lines for inclusive production, assuming a single quark-quark interaction with three spectator quarks

formed to a reference system in which the ratio R of the target momentum to the incident momentum is about equal to 3/2. This ratio is, of course, the ratio of the number of quarks in the target and projectile, it suggests a mechanism with one quark out of each cluster responsible for the collision process, the others remaining passive spectators [47], Fig. 34.

However, serious objections to this simple picture exist. For instance, the ratio R appears to be multiplicity dependent [48], it also depends to some extent on the nature and momentum of the incident particle, (see Fig. 35). Several hypotheses have been proposed to explain the departures from $R = 3/2$: differences between the incoming masses or between the quark masses, quark-quark interactions. The observation of strong K^* production in the reaction studied here gives an opportunity to study if, instead, the difference may be due to resonance production. Indeed, only the pions emitted in the central blob of Fig. 34 may be expected to exhibit the symmetry, not those arising from the decay of a K^* emitted, perhaps, in the same blob.

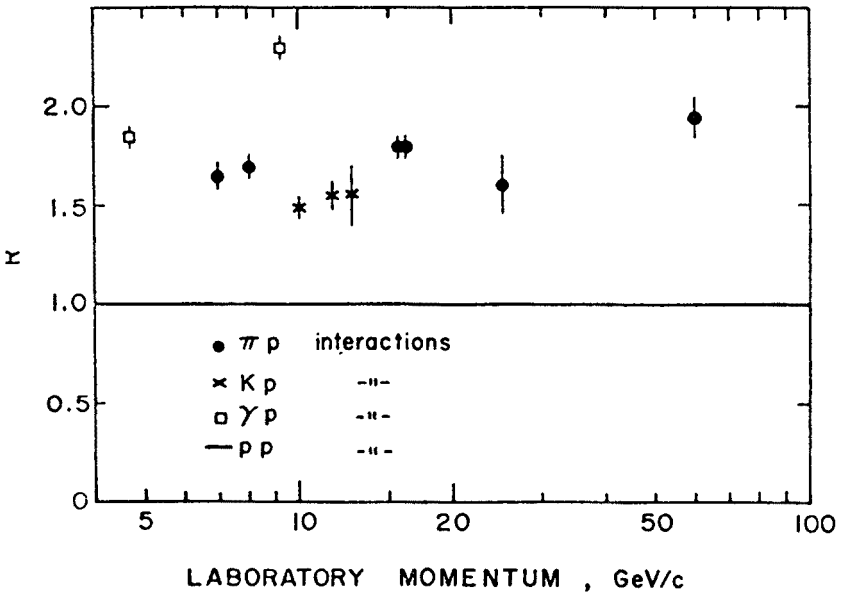

Fig. 35. The ratio R defining the quark-quark collision frame Q, for several incident particles [46]

To separate the contribution of the π^+ arising from K^* decay, a separation was made by fitting the data of Fig. 36 by a K^* signal, represented by a Breit-Wigner, from the background represented by a polynomial, or by an approximate phase-space calculation where adequate. The results are shown by Fig. 37, which shows a) the inclusive π^+ spectra for all π^+, c) for π^+ arising from K^* decay and, by difference, b) for π^+ "directly" produced, as functions of x in the CM system. It is seen that the π^+ spectra, with a maximum in the region $x = 0$, can be well represented both in the forward and backward regions, by exponentials $\exp(-A_{\pm}|x|)$ for $-0.8 < x < 0.8$. The slopes, however, are quite different: for sample b) of "pure" π^+, $A^b_+ = 5.12 \pm 0.10$ (forward) and $A^b_- = 6.82 \pm 0.08$. Although much weaker than for the K^0 (Sect. 3.1), some favoured particle effect is present for the π^+. The transformation to the system with $R = 3/2$ changes the slopes as follows: sample a, $A^a_+ = 5.57 \pm 0.08$, $A^a_- = 5.92 \pm 0.06$, sample b, $A^b_+ = 5.77 \pm 0.10$, $A^b_- = 5.76 \pm 0.06$. Sample b, with the effect of the dominant resonance subtracted, indeed displays a better symmetry, Fig. 38.

These results should also be corrected for the influences of the other resonances abundantly produced: the Q(1320), the $K^*(1420)$, the $\Delta^{++}(1236)$. As the Q decay predominantly *via* $K^*(892)$, most of its effect is already taken into account. The $K^*(1420)$ and Δ^{++} can be shown to give rise to π^+'s with very flat x-spectra, peaking slightly forward and backward respectively, with almost compensating effects.

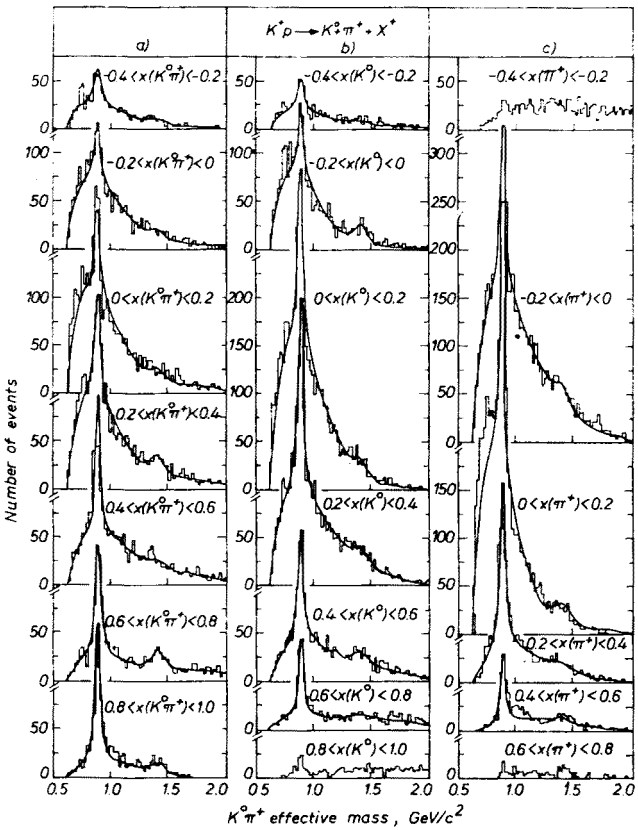

Fig. 36. Effective mass spectra for the reaction $K^+p \to K^0\pi^+X$ (similar to Fig. 28) showing the results of Breit-Wigner + background fits, for several regions of the x variable of the $(K^0\pi^+)$, K^0 and π^+ respectively [49]

Thus one may conclude that, at least in the reaction studied here, a satisfactory symmetry of the directly emitted positive pions is found in the frame of reference of the quark--quark collision.

Recently, Anisovich and Shekhter [50] have attempted, more ambitiously, to use the quark model to predict the relative probabilities of production of different particles at asymptotic energies. They assume that, in the central blob of Fig. 34, quarks are produced which recombined in the SU6 multiplets 36 (mesons) and 56 (baryons), with relative weights given by the corresponding Clebsch-Gordan coefficients, and a unique structure function. The structure function is represented empirically by a function of x and t, with two arbitrary parameters adjusted to the experimental data from $\pi^{\pm}p$ and $K^{\pm}p$ collisions for incident

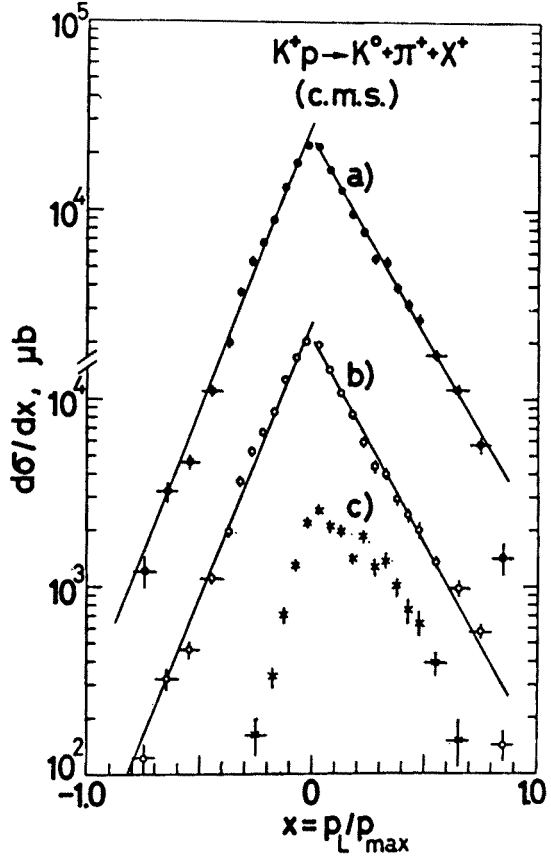

Fig. 37. Inclusive x-spectra for the reaction $K^+p \to K^0\pi^+X^+$ in the CM. a — overall spectrum, b — after subtraction of the π^+ arising from K^* decay, c — spectrum of the π^+ arising from K^* decay [49]

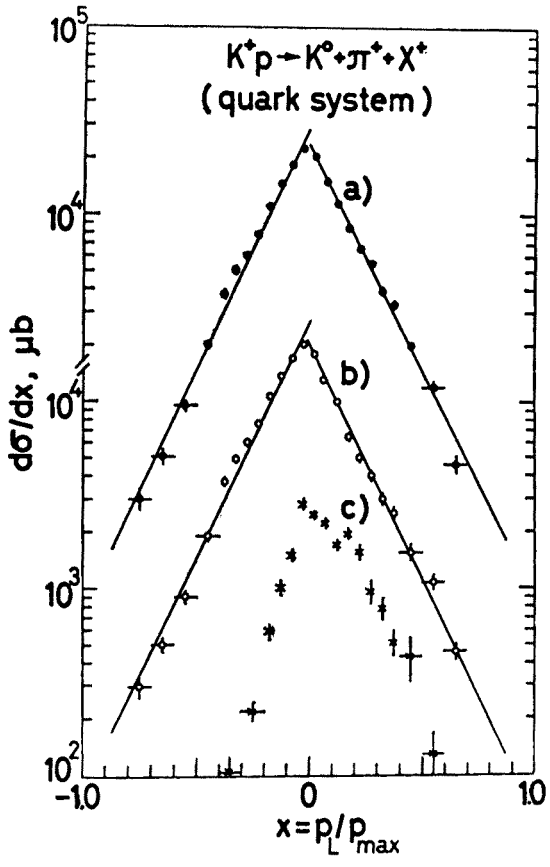

Fig. 38. Similar to Fig. 37, but in the Q system defined by $R = 3/2$

momenta ranging from 8 to 25 GeV/c. A reasonable agreement is found in the region $x = 0.5$ corresponding to the fragmentation of the projectile. In their comparison between model and data, these authors have to assume an isotropic decay of the resonances. With the data presented here, it is possible to make the more detailed comparison of Fig. 39 where

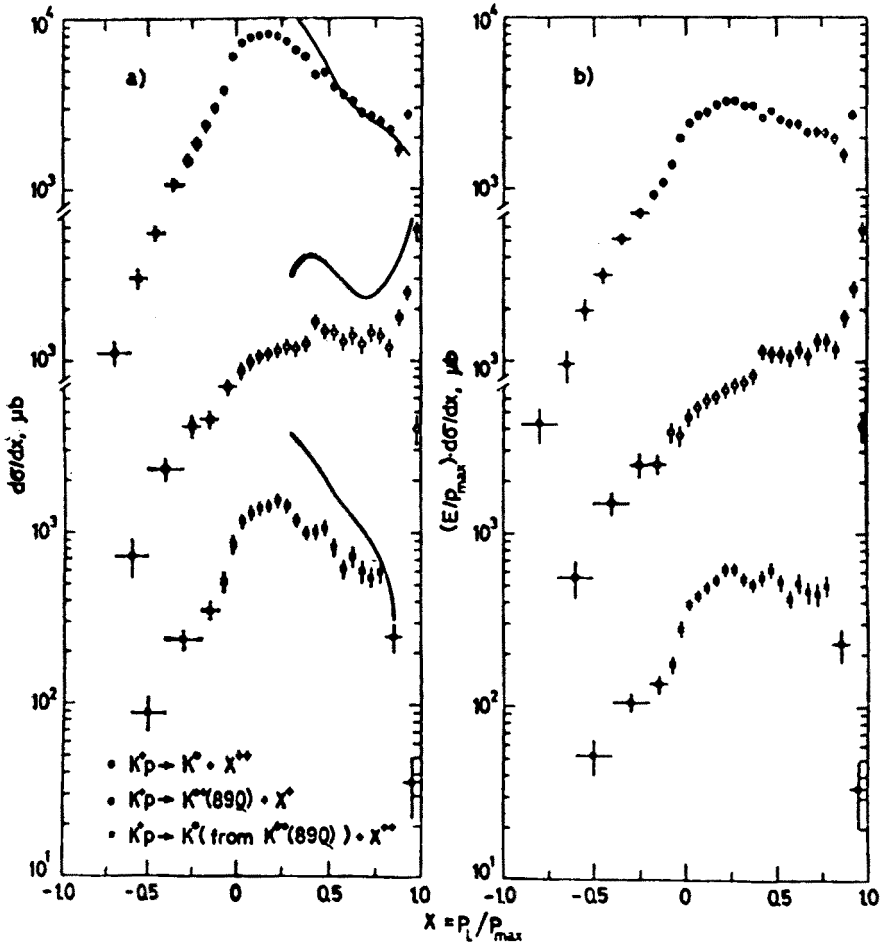

Fig. 39. Predictions of the quark model of Anisovitch and Shekhter [50], compared to the data for the reactions $K^+p \to K^0\pi^+X$ and $K^+p \to K^*\pi^+X$, $K^* \to K^0\pi^+$

the cross-sections for the K^0, K^* and $\bar{K}^0$ arising from K^* decay are shown as functions of x. It is seen that, at least in the forward direction, the K^0 inclusive spectrum shows some agreement with the model. The model predicts a K^* production which is of correct shape, in particular with the forward peak due, as mentioned in Sect. 3.3, to well known exclusive reactions. However, as often the case in quark models, resonance production (K^*) is predicted too high[4].

[4] The author is grateful to K. Zalewski for this remark made at the School.

4. Transverse momenta

4.1. A review

Several prominent properties of the transverse momentum distributions are well known, they may be briefly reviewed and illustrated as follows.

A typical transverse momentum distribution $d\sigma/dp_T$ *vs* p_T is shown by Fig. 40, starting at zero and rising rapidly to a maximum, then decreasing exponentially as p_T

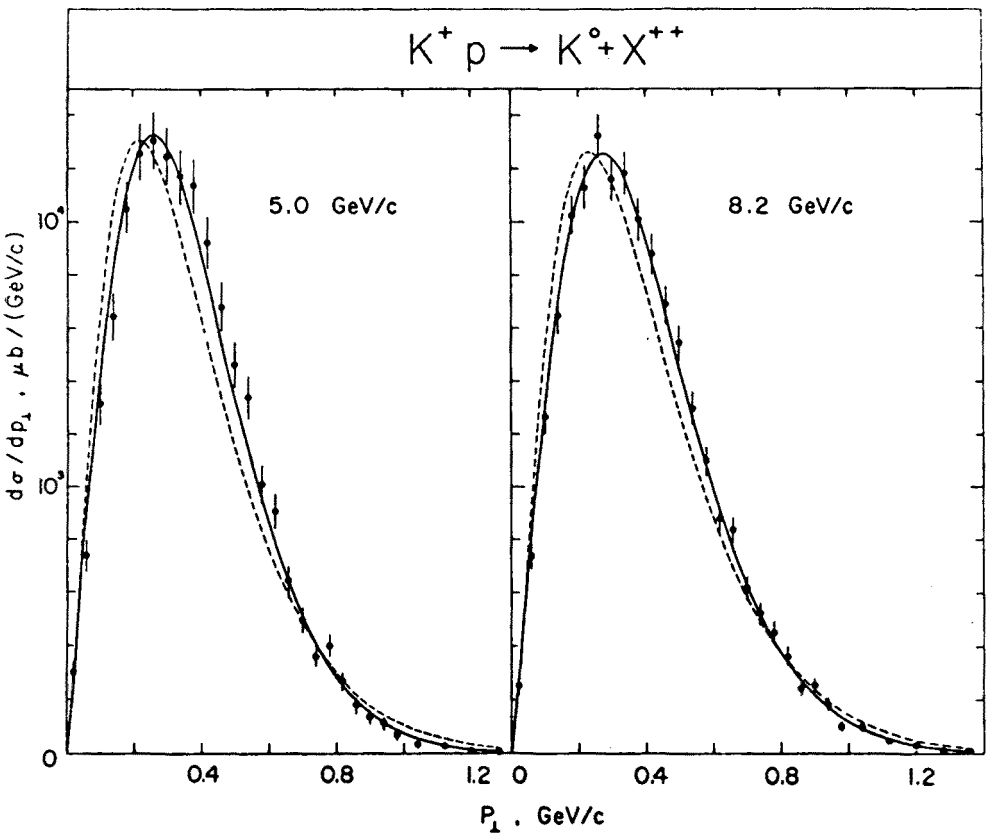

Fig. 40. Transverse momentum p_T distribution for the reaction $K^+p \to K^0X$ at 5 and 8.2 GeV. The lines are results of fits to the Milecin-Rosental formula [60] (full line) and to the Hagedorn [61] formula (dotted line)

increases. The behaviour at small p_T is a phase space effect. Indeed, the plots of the invariant cross-section $Ed\sigma/dp_T^2$ (sometimes called the "weighted" cross-section, *vs* p_T^2 show an almost exponential shape (examples, Fig. 40, 41) but with a definite curvature. In addition, there is a frequent peak for the small values of p_T^2 which has been interpreted as an effect of resonance production [52]. The same quantity $Ed\sigma/dp_T^2$ plotted against p_T (Fig. 42) shows again an almost exponential shape, but now there is a flattening

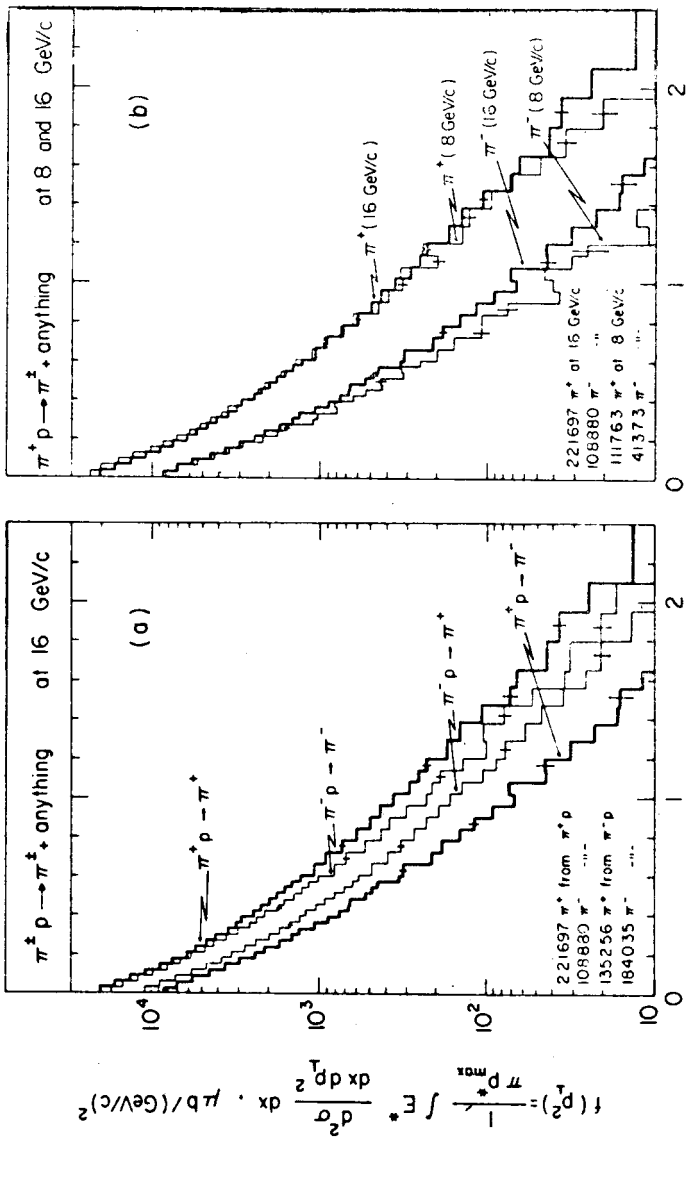

Fig. 41. Invariant cross-section as function of the square of the transverse momentum p_T^2, for the reactions $\pi^* p \to \pi^{\pm} X$ at 8 and 16 GeV [51]

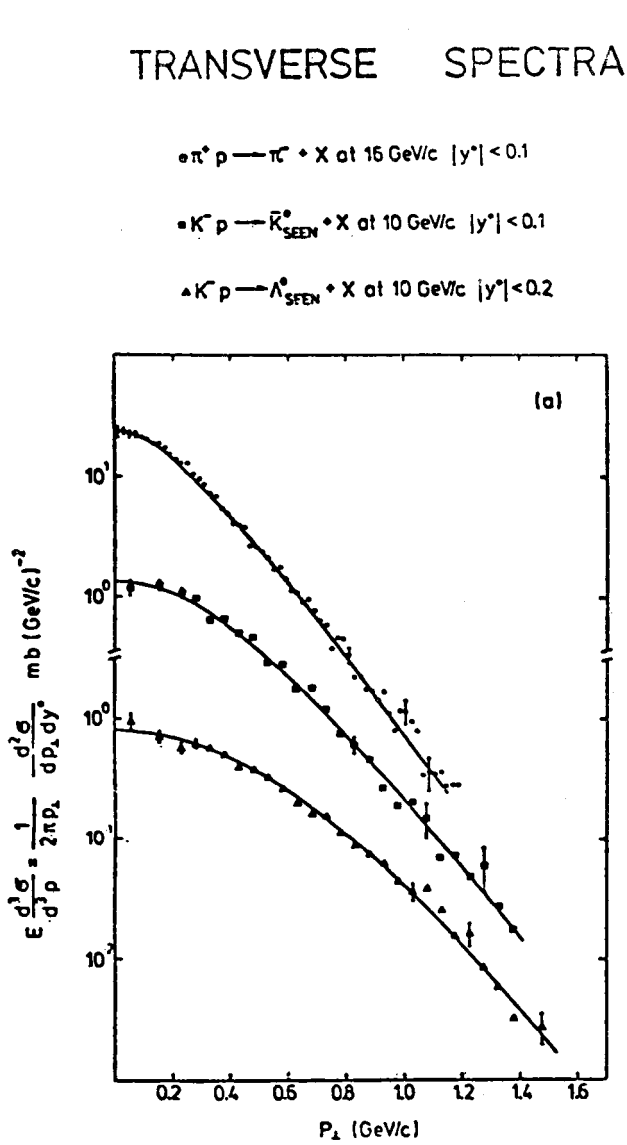

Fig. 42. Invariant cross-section as function of the transverse momentum p_T, for the $\pi^+ p \to \pi^- X$ at 16 GeV, and $K^- p \to \bar{K}^0 X$, $K^- p \to \Lambda^0 X$ at 10 GeV

of the distribution for small p_T. A better representation of the distribution is discussed in Sect. 4.4.

The shape of the transverse momentum distribution depends on p_L. If fitted with an exponential $Ed\sigma/dp_T^2 = A \exp(-bp_T^2)$ over a small region $(0 < p_T < 0.2\ (\mathrm{GeV}/c)^2)$ the slope b, while remaining in the neighbourhood of 6 $(\mathrm{GeV}/c)^2$, shows typical variations shown on Fig. 43 for the reactions $\pi^{\pm} p \to \pi +$anything at 16 GeV/c [51]. As shown by the authors of this experiment, most of these variations may be interpreted as arising from known phenomenon, *i.e.* resonance production and cylindrical phase space.

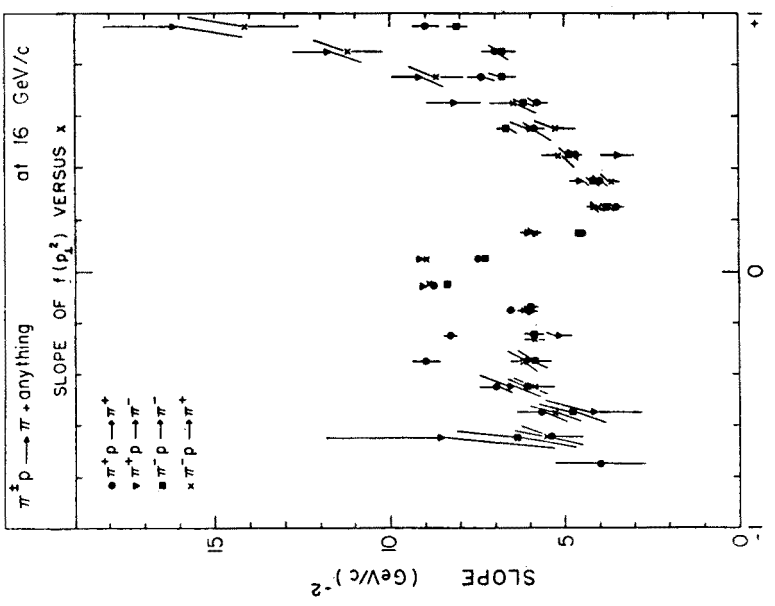

Fig. 43. Slopes of the p_T^2 distribution, as defined in the text, for the reactions $\pi^{\pm}p \to \pi^{\pm}X$ at 16 GeV

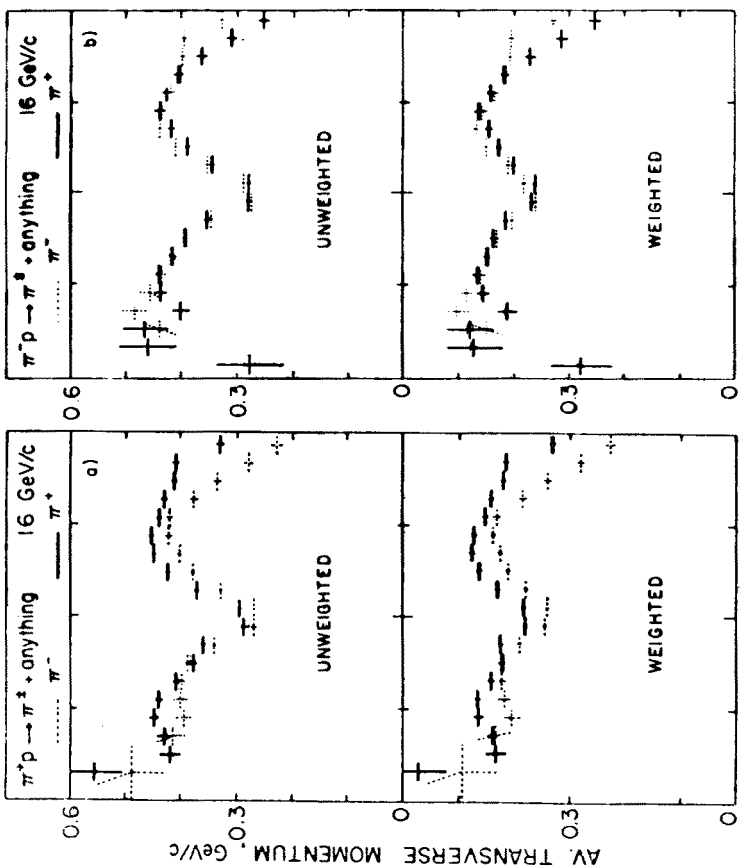

Fig. 44. Average transverse momentum unweighted (6) and weighted (7), for the reactions $\pi^{\pm}p \to \pi^{\pm}X$ at 16 GeV. The seagull effect is reduced by the weighting, but persists

The average transverse momentum

$$\langle p_T(x)\rangle = \frac{\int p_T \frac{d^2\sigma}{dx dp_T^2} dp_T^2}{\int \frac{d^2\sigma}{dx dp_T^2} dp_T^2} \tag{6}$$

is well known to be, in first approximation, an almost universal constant $\langle p_T\rangle \cong 350$ MeV. However, it increases slowly with incident momentum [53] and with the mass of the particle [54]. As a function x or p_L, it shows a characteristic "Polish seagull" [55] shape, Fig. 44. Part of the seagull behaviour is known to originate from the effects of phase space. In particular, if the average is taken instead, with the invariant cross-section ("weighted")

$$\langle p_T^W\rangle = \frac{\int p_T \frac{E d^2\sigma}{dx dp_T^2}}{\int E \frac{d^2\sigma}{dx dp_T^2}} \tag{7}$$

most, but not all of the seagull effect disappears (Fig. 44).

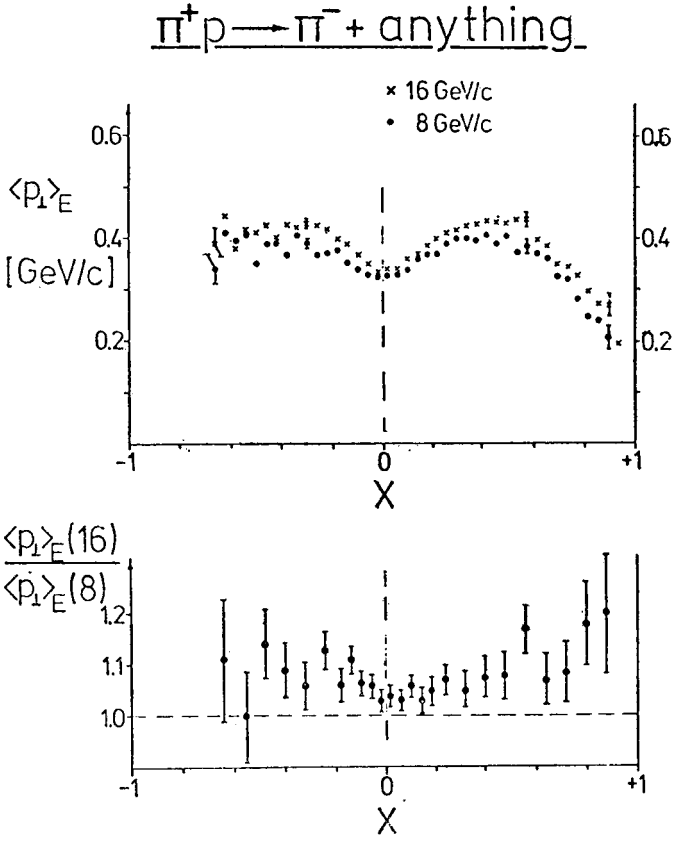

Fig. 45. Average transverse momentum, weighted, for the reaction $\pi^+p \to \pi^-p$ at 8 and 16 GeV. The lower part of the figure shows the ratio of the transverse momenta at 8 and 16 GeV

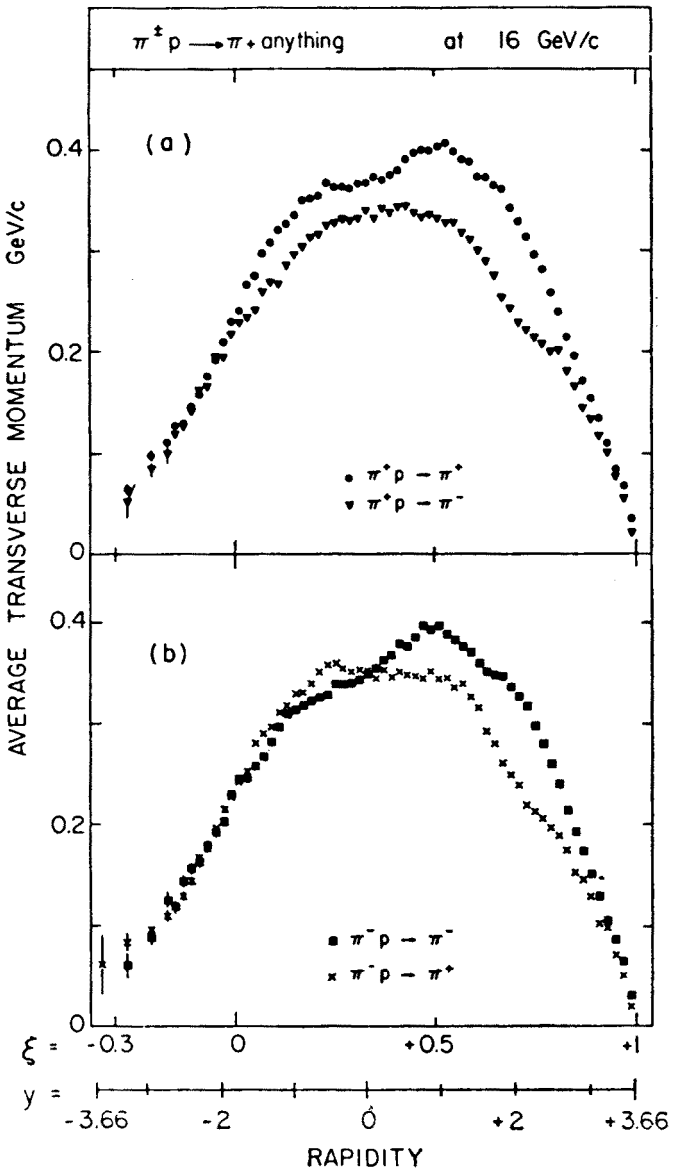

Fig. 46. Average transverse momentum *vs* rapidity for the reactions $\pi^{\pm}p \to \pi^{\pm}X$ at 16 GeV

It is interesting to note that the increase of $\langle p_T \rangle$ with increasing energy is mostly due to the regions of large $|p_L|$; in the words of Deutschmann *et al.* [56] "the seagull distribution raises its wings with increasing beam momentum" (Fig. 45).

4.2. $\langle p_T \rangle$ and rapidity

The ABBCCHW collaboration has shown recently [51] that, plotted against rapidity y instead of p_L, the average transverse momentum $\langle p_T^W \rangle$ has almost a plateau in a relatively

wide central region around $y = 0$, Fig. 46. The existence of a plateau implies that the structure function would then factorize, $f_1(y, p_T) = f_1(y) \cdot \tilde{f}_1(p_T)$. Such factorization is the object of several theoretical speculations [57]. The relation between the rapidity y plot of Fig. 46 and the reduced longitudinal momentum x plot of Fig. 45 may be understood with the help of Fig. 47, which illustrates the kinematical relation between x, p_T and y:

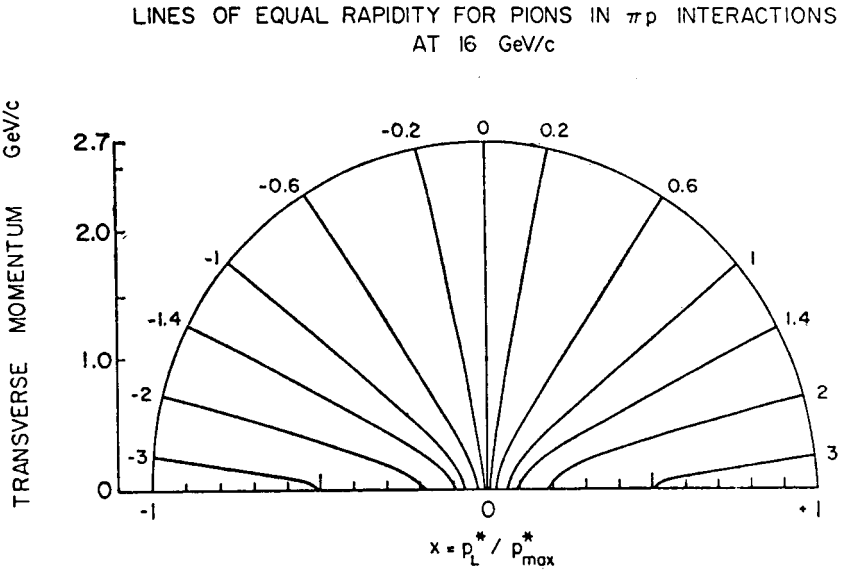

Fig. 47. Kinematic relations between p_L, p_T and y for the reaction $\pi p \to \pi X$ at 16 GeV

one may see how the averaging in y takes place over almost radial regions of the Peyrou plot x, p_T. It is clear also that, for large values of y ($|y| > 1.4$ in this example) the averaging takes place only in regions of small p_T.

4.3. Bose-Einstein parametrization

In a study of K^+p interactions at 11.8 GeV, Erwin *et al.* [58] observe that, the emitted π^-, K^0 and π^+ have an almost isotropic angular distribution for small value of their energy E. The invariant cross-section $Ed^3\sigma/d^3p$, when plotted against E, is found to follow a law of the Bose-Einstein (BE) form

$$\frac{d^3\sigma}{d^3p} = \frac{A}{e^{-E/T} - 1}$$

with $T = 142$ MeV. The departure of the BE shape from an exponential is particularly visible, for small values of E, for the pions. For particles of higher mass, the threshold in E is larger and the distribution becomes practically exponential. Similar results [59] were found at 5 and 8 GeV, also for incident K^+. The angular distributions are shown by Fig. 48, and the corresponding spectrum by Fig. 49.

How are these results related to the transverse momentum distribution? If, indeed, the energy spectrum follows the BE distribution, then Milecin and Rosental [60] have shown by integration over the whole range of p_L, that the transverse momentum spectrum is given by (for $\exp(E_{max}/T) \gg 1$):

$$\frac{d\sigma(p_T)}{dp_T} \sim p_T \sqrt{p_T^2+m^2} \sum_{n=1}^{\infty} K_1(n\sqrt{p_T^2+m^2}/T),$$

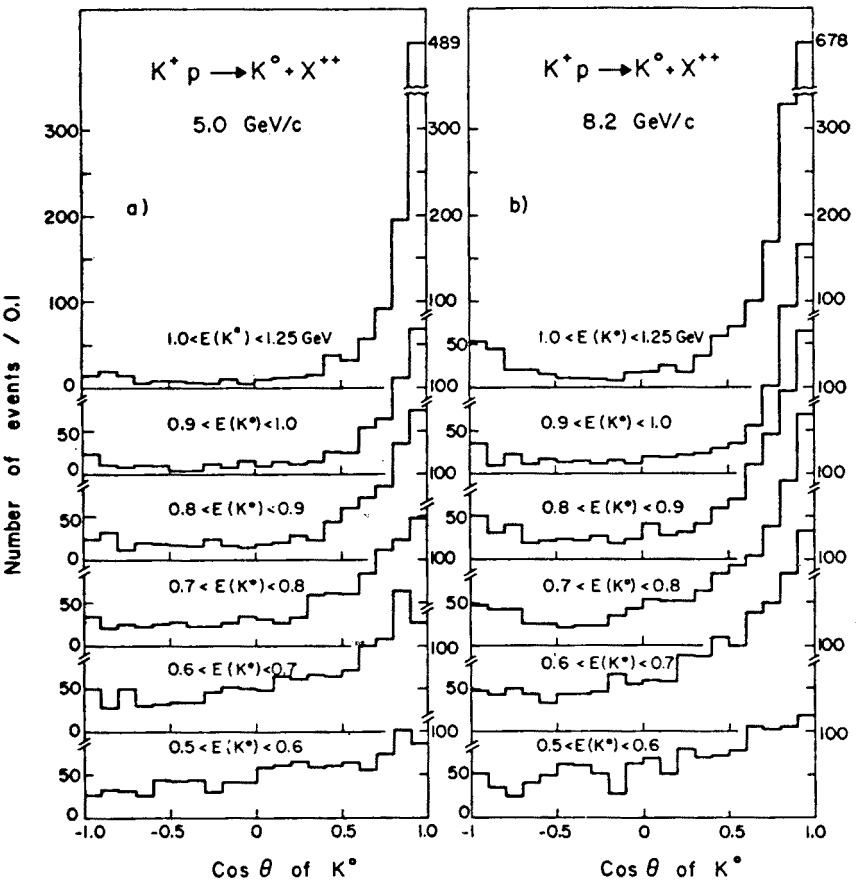

Fig. 48. Angular distribution of the K^0 at 5 and 8.2 GeV, for the reaction $K^+p \to K^0X$, for several intervals of the K^0 energy E [59]

where K_1 is the modified Bessel function of second kind and order 1. The asymptotic form of the first term, for $(\sqrt{p_T^2+m^2}/T) > 1$, gives the often-used Hagedorn formula [61]

$$\frac{d\sigma(p_T)}{dp_T} \sim p_T^{3/2} \exp(-p_T/T).$$

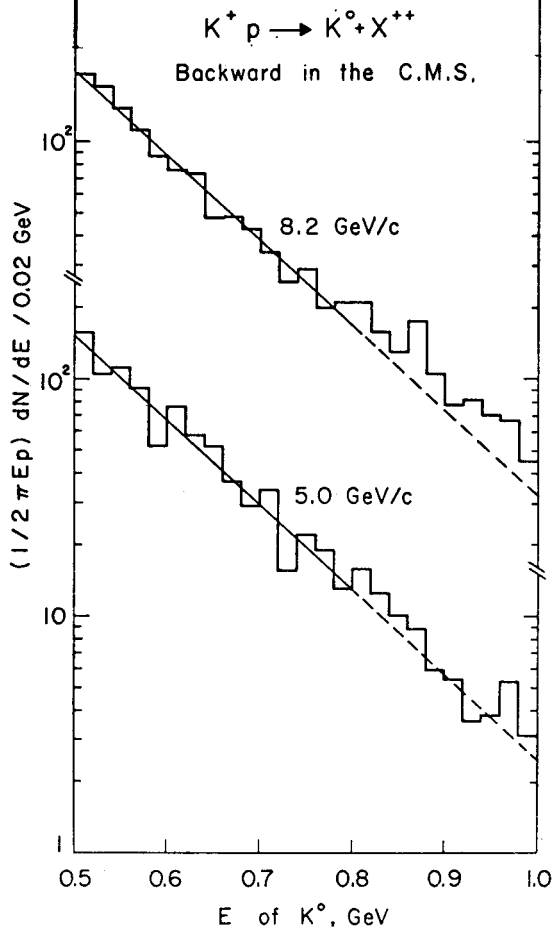

Fig. 49. Spectra of the K^0 of Fig. 49, for the quasi isotropic region $E < 0.8$ GeV. The lines are fits to the Bose-Einstein distribution

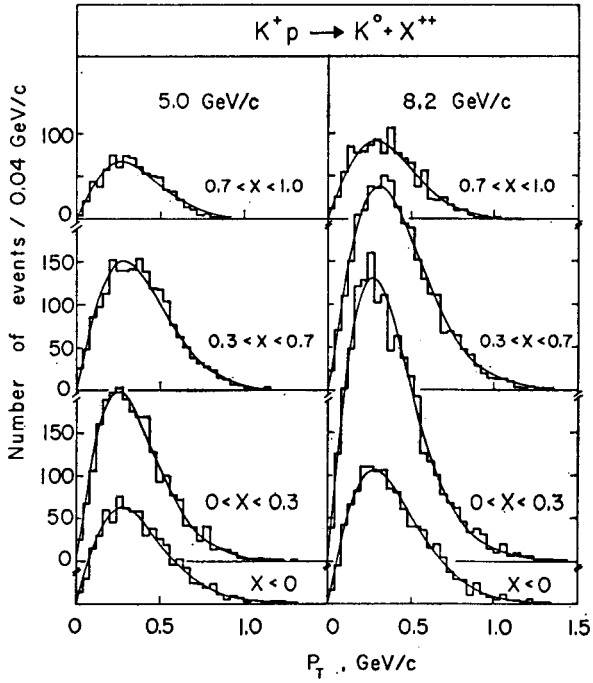

Fig. 50. Transverse momentum spectra of the reaction $K^+p \to K^0X$, at 5 and 8 GeV, for several regions of x. The lines are obtained by integration of the B–E formula. The overall distributions (summed over all x) are given on Fig. 40

These formulae are compared to the experimental results on Fig. 40. It is remarked that, although the BE description may be expected to be valid only in the region of isotropy, for $E < 1$ GeV, the corresponding description of the transverse momentum distribution appears to remain approximately valid for the complete spectrum, regardless of the value of E. A more differential comparison is made in Fig. 50 for different regions of x. The curves are obtained by integration of the BE spectrum in the corresponding region of x.

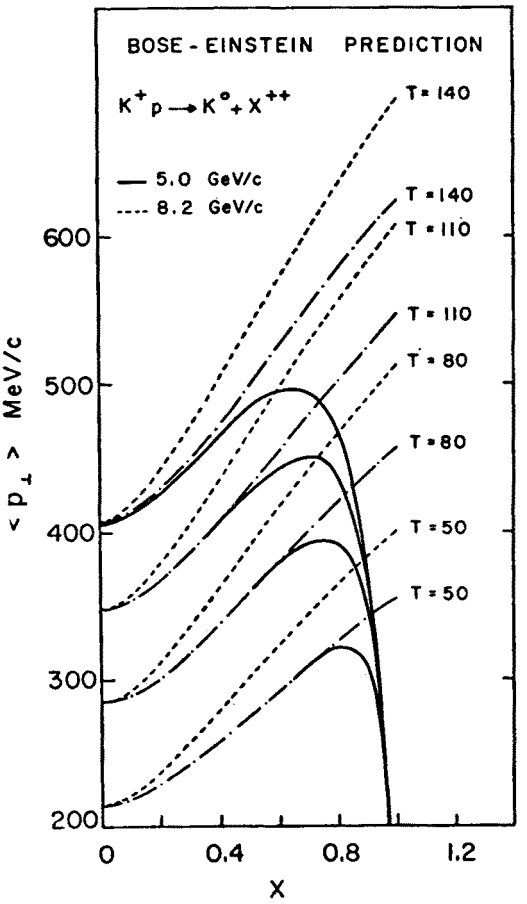

Fig. 51. Average transverse momentum as computed from the BE distribution for the reaction $K^+p \to K^0X$, at 5 GeV, and for different values of T

A more quantitative comparison may be made by examining average values of transverse momenta. The prediction obtained by integrating the BE formula over the available phase space is shown on Fig. 51: a strong seagull effect is predicted, which is not completely followed by the data (Fig. 52). Indeed, if in the backward direction, the BE prediction is good, with $T \cong 120$ MeV, in the forward direction the value of T decreases (Fig. 53). Similar results are found by the ABBCCHLVW collaboration [56]: the value of T, computed

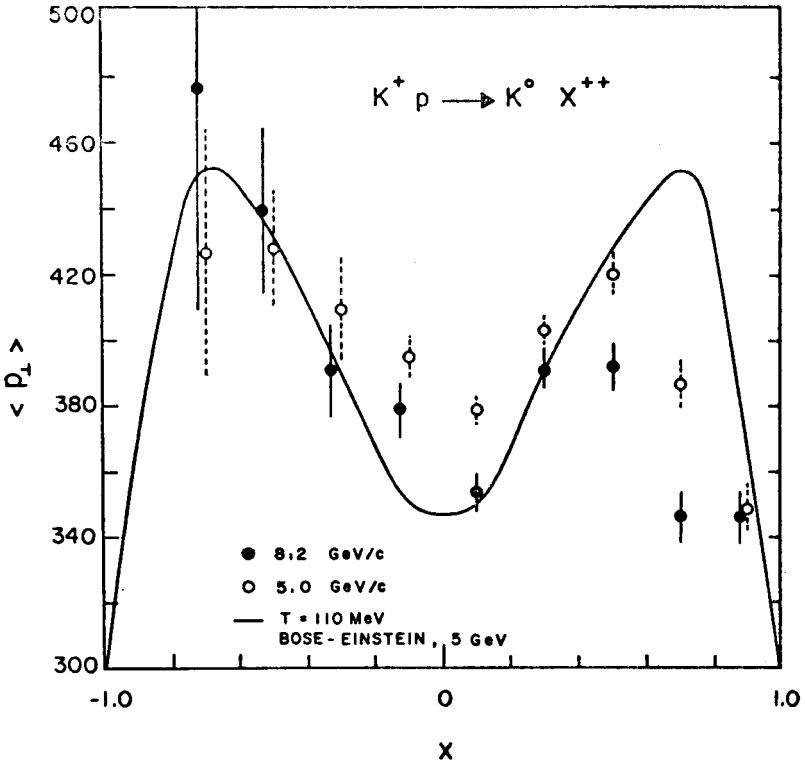

Fig. 52. Observed average transverse momentum, compared to the prediction of Fig. 52. The temperature parameter T of the BE formula is not constant for all values of x (see Fig. 54)

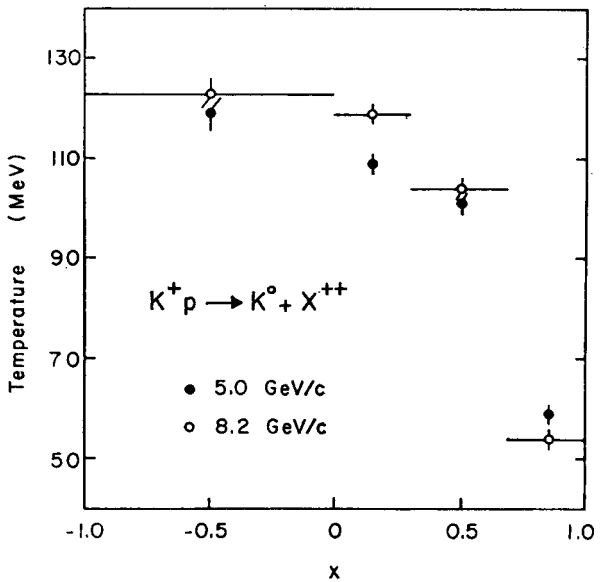

Fig. 53. Observed effective temperature T as function of the production angle Θ, for the reaction $K^+p \to K^0X$ at 5 GeV and 8 GeV

for the almost isotropic part of the angular distribution, $E < 0.32$ GeV, seems to be almost constant in the backward region, but strong changes are observed in the forward hemisphere. Indeed, in this case, the temperature appears to rise there (Fig. 54).

4.4. Average transverse energy *vs* rapidity

If, as shown in the previous Section, the behaviour of the p_T distribution follows the predictions derived from the BE distribution, even outside the region of angular isotropy, then the distribution in E should follow closely an exponential (except perhaps

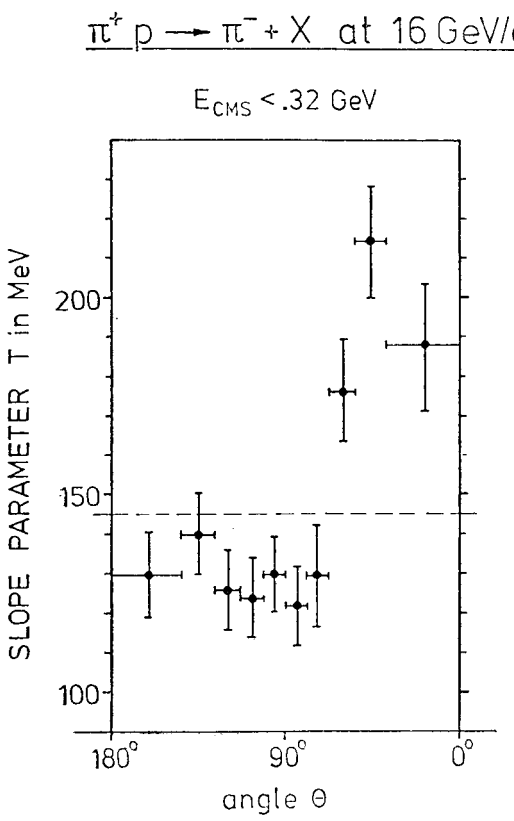

Fig. 54. Observed effective temperature T, as function of the production angle Θ, for the reaction $\pi^- p \to \pi^- X$ at 16 GeV [56]

for small values of E) at least for the region near $x = 0$ in the CM, where $E = \sqrt{m^2 + p_T^2}$. This behaviour is indeed well obeyed by the data, as shown by Fig. 55. It is reported [56] that the fit is better with the non-invariant cross-section $d^3\sigma/d^3p$ than with the invariant cross-section $Ed^3\sigma/d^3p$.

The same behaviour is obtained [56] when the distribution is observed in successive regions of the rapidity y. Indeed, the values of T found in this way, when plotted against y, show an interesting approximate central plateau, Fig. 56. This plateau is directly related

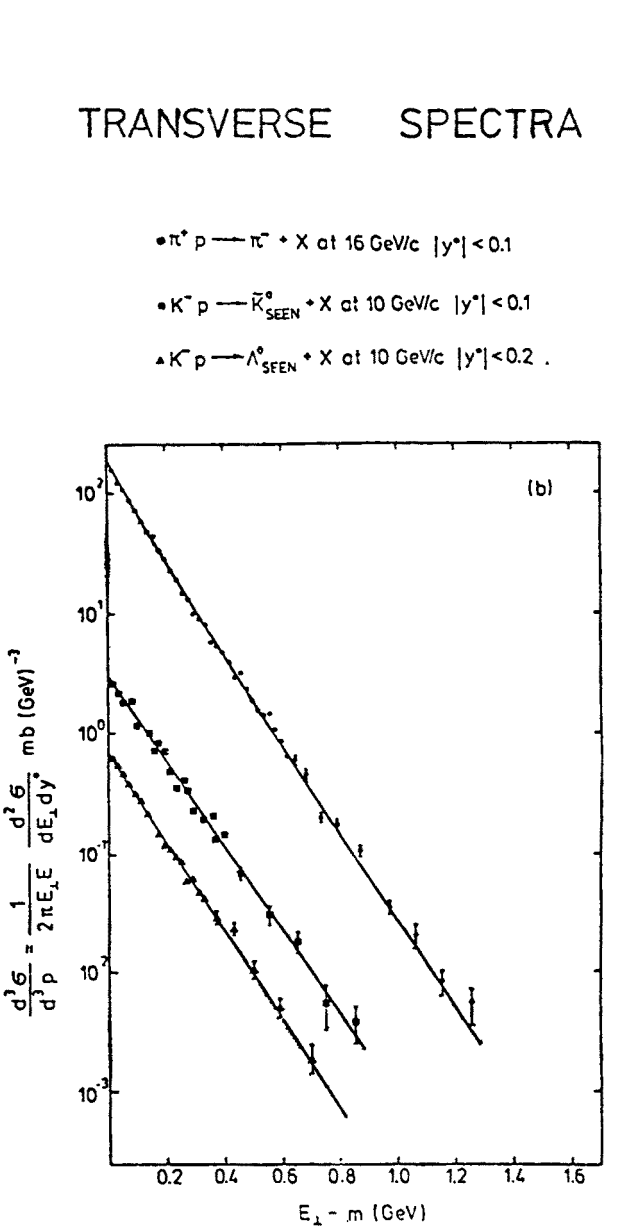

Fig. 55. Distribution of E, in the region near $x = 0$, for the reactions of Fig. 42. The lines represent simple exponentials

to the similar observation for the average transverse momentum $\langle p_T \rangle$ *vs* y presented in Sect. 4.2 and Fig. 46. It should be remembered that each slice in y defines a reference frame in which, again, $E = \sqrt{m^2 + p_T^2}$. In this sense, and with the approximate factorization implied by the presence of plateau-like region in y, one may think in terms of a transverse motion almost independent of the longitudinal motion, occurring near $y = 0$ in successive frames of references moving with different longitudinal velocities.

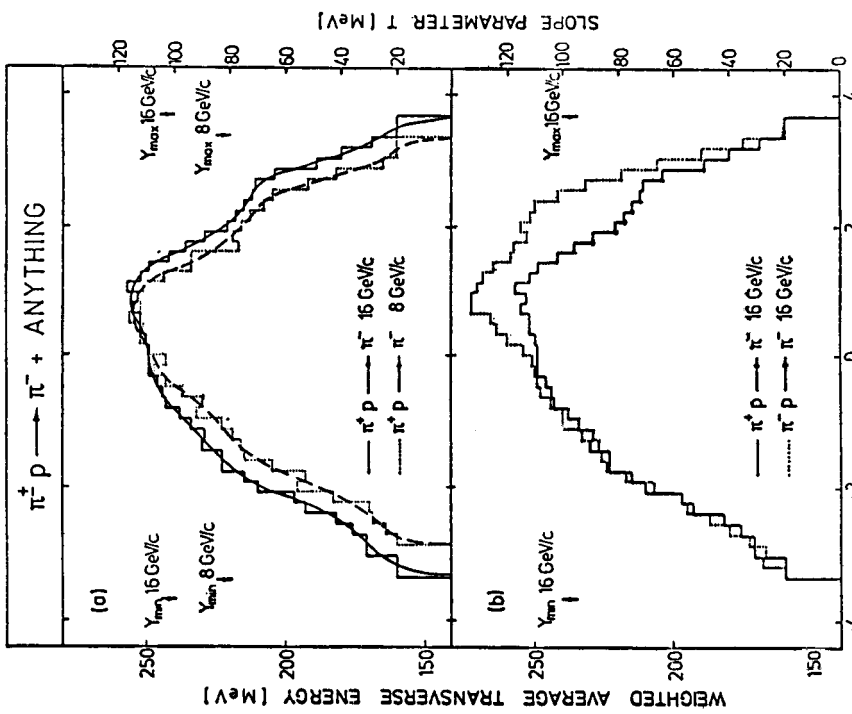

Fig. 56. Observed effective temperature T as function of the rapidity y, for the reactions $\pi^{\pm} p \to \pi^{\pm} X$ at 16 GeV [56]

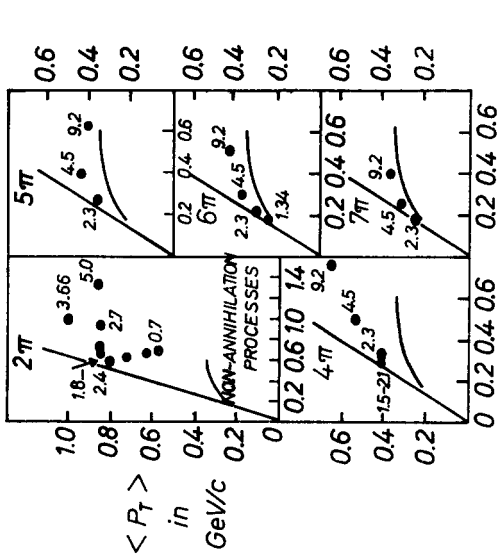

Fig. 57. Average transverse momentum for proton--antiproton annihilation [62]

Detailed comparisons with the predictions of thermodynamical models would be very interesting, but have not yet been reported. Meanwhile, it may be recommended to display the experimental results on transverse distributions as function of E, in successive regions of y.

4.5. Annihilations

The pions emitted by the annihilation of antiprotons show an exceptional behaviour of transverse momentum: the average value is larger than in other high energy collisions and the p_L dependence is different. Gregory *et al.* [62] have shown, see Fig. 57, that the average $\langle p_T \rangle$ plotted against $\langle p_L \rangle$, for different final state multiplicities, is significantly larger than in non-annihilation processes. This behaviour may extend to other baryon exchange processes, as shown by Fry *et al.* [63].

For the second time in these lectures, high energy annihilations show interesting surprises (see Sect. 2.3) underlining the interest of further experiments at higher incident energy.

REFERENCES

[1] R. P. Feynman, *Phys. Rev. Letters*, **23**, 1415 (1969).

[2] J. Benecke, T. T. Chou, C. N. Yang, E. Yen, *Phys. Rev.*, **188**, 2159 (1969).

[3] A. H. Mueller, *Phys. Rev.*, **D2**, 2963 (1970).

[4] H. M. Chan, C. S. Hsue, C. Quigg, J. M. Wang, *Phys. Rev. Letters*, **26**, 672 (1971) and references therein.

[5] W. Kittel, *Review talk given at the Institute of Physics Conference on Elementary Particle Physics*, Southampton, September 1972, CERN/d. Ph. II/PHYS 72-49; *Proceedings of the 1972 CERN School at Grado*, CERN 72-17, p. 227.

[6] D. R. O. Morrison, *Proceedings of the III International Colloquium on Multiparticle Reactions*, Zakopane 1972, Report NR 1421/VI/PH, p. 348, Warsaw 1972, also CERN/D. Ph. II/PHYS 72-25.

[7] G. Goldhaber, S. Goldhaber, W. Lee, A. Pais, *Phys. Rev.*, **120**, 300 (1960).

[8] A. Fridman, *Notions sommaires sur les réactions inclusives à une particule*, Cours à l'Université Louis Pasteur, Strasbourg CBH 72-3 (1972).

[9] R. C. Arnold, *Lectures on Inclusive Reactions*, Argonne 1971, ANL/HEP 7139.

[10] L. Van Hove, *Phys. Reports*, **1C**, 347 (1971).

[11] W. Kittel, *Scandinavian Conference on High Energy Physics*, Spating 1972. Also CERN/D. Ph. II/PHYS 72-11.

[12] W. R. Frazer, L. Ingber, C. H. Mehta, C. H. Poon, D. Silverman, K. Stowe, P. D. Ting, J. J. Yesian, *Rev. Mod. Phys.*, **44**, 284 (1972).

[13] E. L. Berger, *Colloquium on Multiparticle Dynamics*, Helsinki 1971, E. Byckling *et al.*, ed., p. 326. Also Argonne ANL/HEP 7134, Summer 1971, *Workshop on Physics of the 12 foot bubble chamber*, Argonne ANL/HEP 7148.

[14] M. Deutschmann, *Amsterdam International Conference on Elementary Particles*, 1971, A. G. Tanner and J. G. Vettman, Ed., North Holland, Amsterdam 1972, p. 153.

[15] H. M. Chan, *IV International Conference on High Energy Collisions*, Oxford 1972. Also Rutherford RPP/T/17; *Proceedings of the 1972 CERN School at Grado*, CERN 72-17, p. 1. Also Rutherford RPP/T/21.

[16] F. Gliozzi, E. Predazzi, S. Sciuto, *Ecole Internationale de la physique des particules élémentaires*, Basko-Polje-Makarska, Yugoslavia, Strasbourg 1972.

[17] K. Gottfried, *CERN Academic Training Program*, CERN Ref. TH. 1615, 1973.

[18] M. E. Law, J. Kasman, R. S. Panvini, W. H. Sims, T. Ludlam, Particle data group, Lawrence Berkeley Laboratory, LBL-80, August 1962.

[19] M. Boratav, Nguyen Han Khanh, L. P. N. H. E., Paris, 72/03.

[20] M. Jacob, *Proceedings of the XVI International Conference on High Energy Physics*, 1972, J. D. Jackson and A. Roberts, Ed., National Accelerator Laboratory, Batavia 1973, vol. 3, p. 373.

[21] V. V. Ammosov, J. P. Baton, P. Beillière, P. Bosetti, V. A. Bumazshnov, M. Czejthey-Barth, D. P. Dallman, A. Daudin, B. Deler, N. G. Demidov, T. W. Dombeck, P. Duinker, P.F. Ermolov, A. B. Fenyuk, P. A. Gorichev, F. Grard, H. Grässler, S. A. Gumenyuk, Ph. Herquet, G. Kellner, J. Kesteman, E. P. Kistenev, W. Kittel, V. M. Kubik, D. Kuhn, K. Lanius, J. Laurent, A. Meyer, B. A. Manyukov, A. M. Moiseev, D. R. O. Morrison, L. Mosca, M. Neveu, V. M. Perevozchikov, R. Pose, J. Schlesinger, R. M. Sulyaev, P. R. Thornton, F. Triantis, F. Verbeure, A. P. Vorobjev, R. Windmolders, M2, CERN/D. Ph. II/PHYS 73–5, *Nuclear Phys.* (in the press).

[22] J. N. Carney, D. C. Colley, M. Jobes, J. B. Kinson, M. Storr, S. K. Tuli, D. Watkins, W. De Baere, E. De Wolf, F. Grard, P. Herquet, P. Peeters, F. Verbeure, R. Windmolders, C. Bouthet, J. Ginestet, D. Manesse, Tran Ha Anh, D. Vignaud, M. Sené, G. Ciapetti, W. Dunwoodie, R. L. Eisner, Y. Goldschmidt-Clermont, A. Grant, V. P. Henri, F. Muller, L. Pape, J. Quinquard, Z. Sekera, J. Tuominiemi, N. Yamdagni and private communication from W. Dunwoodie and J. Tuominiemi. Paper in preparation.

[23] S. L. Stone, D. Cohen, M. Farber, T. Ferbel, R. Holmes, P. Slattery, B. Werner, *Nuclear Phys.*, **B32**, 19 (1971).

[24] D. B. Smith, *Ph. D. Thesis*, University of California, Berkeley, UCRL 20632, 1971.

[25] D. R. O. Morrison, *Review Lecture at the Royal Society Meeting on Proton-Proton Scattering at Very High Energies*, London 1973, CERN/D. Ph. II/PHYS 73–11.

[26] H. Satz, *Nuovo Cimento*, **37**, 1407 (1965); A. Krzywicki, *Nuovo Cimento*, **32**, 1067 (1964).

[27] E. L. Berger, A. Krzywicki, *Phys. Letters*, **36B**, 380 (1971).

[28] P. Söding, Lectures given at this School.

[29] A. Wróblewski, *Proceedings of the XV International Conference on High Energy Physics*, Kiev 1971, V. Shelest et al., ed., Naukova Dumka, Kiev 1972, p. 42.

[30] See ref. [20], [31] and references therein.

[31] D. Drijard, S. Pokorski, *Phys. Letters*, **43B**, 509 (1973) and references therein.

[32] B. R. Webber, *Phys. Letters*, **42B**, 69 (1972).

[33] A. Wróblewski, *Proceedings of the III International Colloqium on Multiparticle Reactions*, Zakopane 1972, Report NR 1421/VI/PH, Warsaw 1972, p. 140.

[34] Z. Koba, H. B. Nielsen, P. Olesen, *Nuclear Phys.*, **B40**, 317 (1972).

[35] A. Białas, *Proceedings of the III International Colloquium on Multiparticle Reactions*, Zakopane 1972, Report NR 1421/VI/PH, Warsaw 1972, p. 414.

[36] O. Czyżewski, K. Rybicki, *Nuclear Phys.*, **B47**, 633 (1972).

[37] C. P. Wang, *Phys. Rev.*, **180**, 1463 (1971).

[38] J. V. Beaupré, M. Deutschmann, H. Grässler, P. Schmitz, U. Gensch, W. D. Nowak, H. J. Schreiber, M. Walter, E. De Wolf, F. Grard, P. Herquet, L. Pape, P. Peeters, F. Verbeure, R. Windmolders, A. Angelopoulos, P. V. Chliapnikov, V. T. Cocconi, O. Czyżewski, D. Drijard, P. Duinker, W. Dunwoodie, A. Eskreys, Y. Goldschmidt-Clermont, A. Grant, J. D. Hansen, V. P. Henri, W. Kittel, D. Linglin, S. Matsumoto, J. Meyer, D. R. O. Morrison, F. Muller, S. Nielsen, Z. Sekera, R. Stroynowski, P. J. Dornan, G. A. Grammatikakis, B. R. Kumar, A. Mutalib, B. Buschbeck, A. Froelich, P. Porth, H. Wahl, *Nuclear Phys.*, **B30**, 381 (1971); see also P. V. Chliapnikov, S. Nielsen, G. Ciapetti, D. Drijard, W. Dunwoodie, Y. Goldschmidt-Clermont, A. Grant, V. P. Henri, F. Muller, L. Pape, Z. Sekera, W. De Baere, W. De Wolf, F. Grard, P. Herquet, P. Peeters, F. Verbeure, R. Windmolders, N. C. Carney, D. C. Colley, M. Jobes, G. T. Jones, C. Bonnel, J. Ginestet, D. Manesse, Tran Ha Anh, D. Vignaud, M. Sené, *Phys. Letters*, **39B**, 279 (1972).

[39] W. De Baere, J. Debaisieux, P. Dufour, F. Grard, J. Heughebaert, L. Pape, P. Peeters, F. Verbeure, R. Windmolders, G. Bassompierre, D. Drijard, Y. Goldschmidt-Clermont, A. Grant, V. P. Henri, B. Jongejans, D. Linglin, F. Muller, J. M. Perreau, H. Piotrowska, I. Saitov, R. Sekulin, G. Wolf, paper presented at the Vienna Conference 1968.

[40] H. I. Miettinen, *Phys. Letters*, **38B**, 431 (1972).

[41] P. Chliapnikov, O. Czyżewski, M. Jacob, F. Finkelstein, *Phys. Letters*, **35B**, 581 (1971).

[42] P. Chliapnikov, O. Czyżewski, Y. Goldschmidt-Clermont, M. Jacob, P. Herquet, *Nuclear Phys.*, **B37**, 336 (1972).

[43] J. N. Carney, D. C. Colley, M. Jobes, J. B. Kinson, M. Storr, S. K. Tuli, D. Watkins, W. De Baere, E. De Wolf, F. Grard, P. Herquet, P. Peeters, F. Verbeure, R. Windmolders, C. Bouthet, J. Ginestet, D. Manesse, Tran Ha Anh, D. Vignaud, M. Sené, G. Ciapetti, W. Dunwoodie, R. L. Eisner, Y. Goldschmidt-Clermont, A. Grant, V. P. Henri, F. Muller, L. Pape, J. Quinquard, Z. Sekera, J. Tuominiemi, N. Yamdagni, *Phys. Letters*, **42B**, 124 (1972).

[44] K. Buchner, G. Dehm, G. Goebel, H. Hupe, W. Wittek, G. Wolf, Y. Goldschmidt-Clermont, A. Grant, V. P. Henri, G. De Jongh, P. Dufour, F. Grard, J. Heughebaert, S. Tavernier, G. Thill, R. Windmolders, *Nuclear Phys.*, **B29**, 381 (1971).

[45] P. Estabrooks, A. D. Martin, *Phys. Letters*, **42B**, 229 (1972); C. Michael, TH 1627 CERN, submitted to *Nuclear Phys.* and references therein.

[46] K. Boesebeck, M. Deutschmann, M. Matziolis, R. Speth, V. Kundt, H. Nowak, K. Böckmann, R. Hartmann, Ch. Kanazirsky, H. Schachter, T. Besliu, V. T. Cocconi, P. F. Dalpiaz, P. Duinker, W. Kittel, D. R. O. Morrison, R. Stroynowski, H. Wahl, A. Eskreys, S. Zaorska, R. Blaschke, A. A. Azoog, M. J. Counihan, J. Hödl, M. Markytan, S. Otwinowski, M. Szeptycka, *Nuclear Phys.*, **B46**, 371 (1972).

[47] E. M. Levin, L. L. Frankfurt, *Zh. Eksper. Teor. Fiz. Pisma*, **2**, 105 (1965). Translation: *JETP Letters*, **2**, 65 (1965); H. J. Lipkin, F. Scheck, *Phys. Rev. Letters*, **16**, 71 (1966); H. Satz, *Phys. Letters*, **25B**, 220 (1967).

[48] J. E. Elbert, A. R. Erwin, W. D. Walker, *Phys. Rev.*, **D3**, 2042 (1971).

[49] P. V. Chliapnikov, L. N. Gerdyukov, B. A. Manyukov, F. Grard, V. P. Henri, Ph. Herquet, R. Windmolders, F. Verbeure, G. Ciapetti, D. Drijard, W. Dunwoodie, Y. Goldschmidt-Clermont, A. Grant, S. Nielsen, L. Pape, Z. Sekera, J. Touminiemi, N. Yamdagni, in preparation. Private communication.

[50] V. V. Anisovich, V. M. Shekhter, *Nuclear Phys.*, **B55**, 455 (1973); N. V. Anisovich, M. N. Kobrinsky, A. K. Likhoded, V. M. Shekhter, *Nuclear Phys.*, **B55**, 474 (1973).

[51] P. Bosetti, H. Grässler, H. Kirk, M. Matziolis, U. Gensch, P. Kostka, K. Böckmann, G. J. Bossen, J. Lowsky, M. Rost, T. Besliu, V. T. Cocconi, P. F. Dalpiaz, P. Duinker, S. Matsumoto, D. R. O. Morrison, R. Stroynowski, H. Wahl, T. Coghen, W. Zieliński, S. Brandt, M. Bardadin-Otwinowska, T. Hofmokl, *Nuclear Phys.*, **B54**, 141 (1973). See also CERN/D. Ph. II/PHYS 72-39.

[52] E. Yen, E. L. Berger, *Phys. Rev. Letters*, **24**, 695 (1970).

[53] D. B. Smith, R. J. Sprafka, J. A. Anderson, *Phys. Rev. Letters*, **23**, 1064 (1969).

[54] J. Bartke, W. A. Cooper, B. Czapp, H. Filthuth, Y. Goldschmidt-Clermont, L. Montanet, D. R. O. Morrison, S. Nilsson, Ch. Peyrou, R. Sosnowski, A. Bigi, R. Carrara, C. Franzinetti, I. Mannelli, *Nuovo Cimento*, **29**, 8 (1963).

[55] M. Bardadin, *Proceedings of the 1963 Sienna Conference on Elementary Particles*, vol. I, p. 628. Also Institute of Nuclear Research, Warsaw, *Report* 511/VI (1964).

[56] M. Deutschmann, H. Grässler, H. Kirk, P. Sixel, R. Speth, W. Sturm, G. J. Bossen, E. Propach, M. Rost, B. U. Stöcker, T. Besliu, P. Dalpiaz, D. R. O. Morrison, R. Stroynowski, H. Wahl, J. Zaorska, R. Blaschke, S. Brandt and ABBCCHLVW Collaboration, private communication. See also J. T. Powers, N. N. Biswas, N. M. Casou, V. P. Kenney, W. D. Shephard, University of Notre Dame *preprint*, submitted to *Phys. Rev.*

[57] N. F. Bali, L. S. Brown, R. D. Peccei, A. Pignotti, *Phys. Rev. Letters*, **27**, 557 (1970); H. Bøggild, K. H. Hansen, M. Suk, *Nuclear Phys.*, **B27**, 1 (1971); S. Stone, T. Ferbel, P. Slattery, B. Werner, *Phys. Rev.*, **D5**, 1621 (1972).

[58] J. Erwin, W. Ko, R. L. Lander, D. E. Pellett, P. M. Yager, *Phys. Rev. Letters*, **27**, 1534 (1971).

[59] P. V. Chliapnikov, G. Ciapetti, D. Drijard, W. Dunwoodie, P. Eberhard, Y. Goldschmidt-Clermont, V. Henri, A. Grant, D. Linglin, J. Quinquard, J. Nielsen, L. Pape, Z. Sekera, S. Tanaka, N. Yamdagni, W. De Baere, E. De Wolf, F. Grard, P. Herquet, P. Peeters, F. Verbeure, R. Windmolders, CERN/D. Ph. II/72–15 (in preparation). Also P. Chliapnikov, *Thesis*, IPVE (Serpukhov) 72–109.

[60] G. A. Milecin, I. L. Rosental, *Suppl. Nuovo Cimento*, **8**, 770 (1958).

[61] R. Hagedorn, *Suppl. Nuovo Cimento*, **3**, 147 (1965).

[62] P. S. Gregory, P. Grossmann, P. Mason, H. Muirhead, S. O. Holmgren, N. K. Yamdagni, *Phys. Letters*, **43B**, 228 (1973).

[63] J. R. Fry, C. Brankin, H. Muirhead, R. Matthews, A. Angelopoulos, A. Apostolakis, A. Stergiou, P. Theocharopoulos, G. Vasiliades, T. A. Filippas, E. Simopoulou, P. Tsimiligras, A. Vayaki, E. Zevgalatakos, J. Hoedl, D. Kuhn, M. Markytan, G. Otter, H. Rohringer, *Phys. Letters*, **41B**, 539 (1972).